16-week-old MCK-fukutin-cKO mice was significantly higher than that in controls (Fig. 1D). These pathological features were not observed in 8-week-old mice (Fig. 1C and D); a possible reason may be the presence of residual α-DG with proper glycosylation (Supplementary Material, Fig. S2B). The population of myofibers with centrally located nuclei, an indication of repeated cycles of myofiber degeneration/regeneration, increased with age (Fig. 1E); however, more advanced pathology, such as infiltration of fat and connective tissues, was rarely observed even in 48-week-old MCK-fukutin-cKO mice (Fig. 1C).

It has been widely believed that functional and/or substantial loss of DG-containing protein complexes (i.e. the dystrophin–glycoprotein complex) leads to disease-causing membrane fragility. This concept is based on results of forced exercise experiments in animals with muscular dystrophy, which led to increases in the serum CK levels and uptake of membrane-impermeable Evans blue dye by myofibers (26,27). However, these experiments were conducted in diseased animals; therefore, it remains unclear whether membrane fragility triggers disease-causing phenotype. Therefore, we subjected 10-week-old MCK-fukutin-cKO mice, which showed abnormal α-DG modification but no pathology (Supplementary Material, Fig. S2C), to forced exercise. After forced exercise, serum CK levels were dramatically increased in the MCK-fukutin-cKO mice but not in the control mice (Fig. 1F). Myofibers with membrane-impermeable Evans blue dye uptake were also observed only in the exercise-administered MCK-fukutin-cKO mice (Fig. 1G). These data indicate that the plasma membrane of the muscle cells becomes weak before disease onset, providing proof-of-principle that membrane fragility triggers disease manifestation.

Characterization of MPC-selective fukutin cKO mice

Loss of fukutin in differentiated myofibers results in only mild and slow-progressing disease-causing phenotypes. We hypothesized that fukutin-dependent modification also plays a role in MPCs that are not targeted by MCK-Cre-mediated recombination. Therefore, we generated cKO mice lacking fukutin in MPCs by crossing flox fukutin mice with Myf5-Cre knock-in mice (23) 'expressing Cre recombinase under the control of the endogenous Myf5 promoter (Myf5-fukutin-cKO mice; Supplementary Material, Fig. S1). It has been reported that the Myf5-Cre allele recapitulates the expression pattern of the endogenous Myf5 gene and is uniformly expressed in all proliferating myoblasts (23). The Myf5-fukutin-cKO mice grossly show little difference compared with the litter controls until ~2 weeks of age; thereafter, increase in body weight was significantly retarded (Fig. 2A). Most Myf5-fukutin-cKO mice died by 6 months (Fig. 2B). Reduction in fukutin protein expression and abnormal modification were confirmed by immunofluorescence, western blotting, HF treatment and IMAC-bead assay (Fig. 2C and D). As is the case of MCK-fukutin-cKO, α-DG in Myf5-fukutin-cKO localizes to the sarcolemma (Supplementary Material, Fig. S2D). H&E staining revealed progressive pathological changes in Myf5-fukutin-cKO skeletal muscles (Fig. 2E). At 2 weeks, myonecrotic fibers were sparse (Supplementary Material, Fig. S2E), and at 4 weeks, in addition to myonecrotic fibers, myofibers with centrally located nuclei were observed (Fig. 2E). Serum CK levels and the proportion of the myofibers with centrally located nuclei were significantly higher in Myf5-fukutin-cKO mice than in the controls at 4, 8 and 16 weeks (Fig. 2F and G). Sixteen-week-old Myf5-fukutin-cKO mice showed more advanced pathological changes, such as fiber size variation and fibrosis (Fig. 2E). A few specimens showed milder phenotypic changes accompanied by increases in the normally glycosylated α-DG population (Supplementary Material, Fig. S2F). Overall, different phenotypes of the MCK-fukutin-cKO and Myf5-fukutin-cKO mice suggested a pathophysiological role of fukutin-dependent modification in MPCs.

Impaired viability of MPCs in Myf5-fukutin-cKO mice

To determine the impact of fukutin deficiency on MPC activity, we isolated SM/C-2.6(+) satellite cells from young (slightly affected) and adult (diseased) Myf5-fukutin-cKO muscles and then cultured them as MPCs (i.e. myoblasts) (28). The number of isolated SM/C-2.6(+) cells tended to be less in young fukutin-deficient muscles and was significantly reduced in adults compared with the litter controls (Fig. 3A). The proliferation activity of the isolated MPCs was slightly but significantly decreased in young and severely reduced in adult Myf5-fukutin-cKO muscles (Fig. 3B). The differentiation activity of fukutin-deficient myoblasts was significantly lower than that of the control mice (Fig. 3C). Quantification of the Pax7 immunofluorescence signal, a satellite cell marker, on skeletal muscle sections also suggested decreases in the number of satellite cells in adult Myf5-fukutin-cKO mice compared with control mice (Supplementary Material, Fig. S3A). We also examined the population of activated satellite cells by Pax7/MyoD double staining on the skeletal muscle sections from Myf5-fukutin-cKO mice. The results suggested that the number of active satellite cells was reduced in 16-week-old Myf5-fukutin-cKO mice compared with that in 8-week-old Myf5-fukutin-cKO mice (Supplementary Material, Fig. S3B). These data suggest that in addition to decreases in the number of satellite cells, the activation state of satellite cells is impaired in Myf5-cKO mice as the disease progresses.

We next examined *in vivo* regeneration capability of the Myf5-fuktuin-cKO muscles after cardiotoxin (CTX)-induced muscle degeneration. After 14 days of the CTX challenge in adult mice (~3 months old), we observed that the proportion of small myofibers was strikingly higher in Myf5-fukutin-cKO mice than in the controls (Fig. 3D and E). In some cases, the CTX-injected Myf5-fukutin-cKO muscles showed severe atrophic changes compared with the contralateral saline-injected ones (Supplementary Material, Fig. S3C). In younger (~4 weeks old) Myf5-fukutin-cKO mice, after 14 days of the CTX challenge, no obvious histological difference was noted compared with the controls (Supplementary Material, Fig. S3D); however, after 5 days of the CTX challenge, the proportion of smaller regenerating fibers (that are embryonic myosin-positive) was higher in Myf5-fukutin-cKO muscles than in the controls (Supplementary Material, Fig. S3E and F). These minor impairments in the regeneration of younger Myf5-fukutin-cKO skeletal muscles are consistent with the *in vitro* results. Overall, our data showed that fukutin-dependent

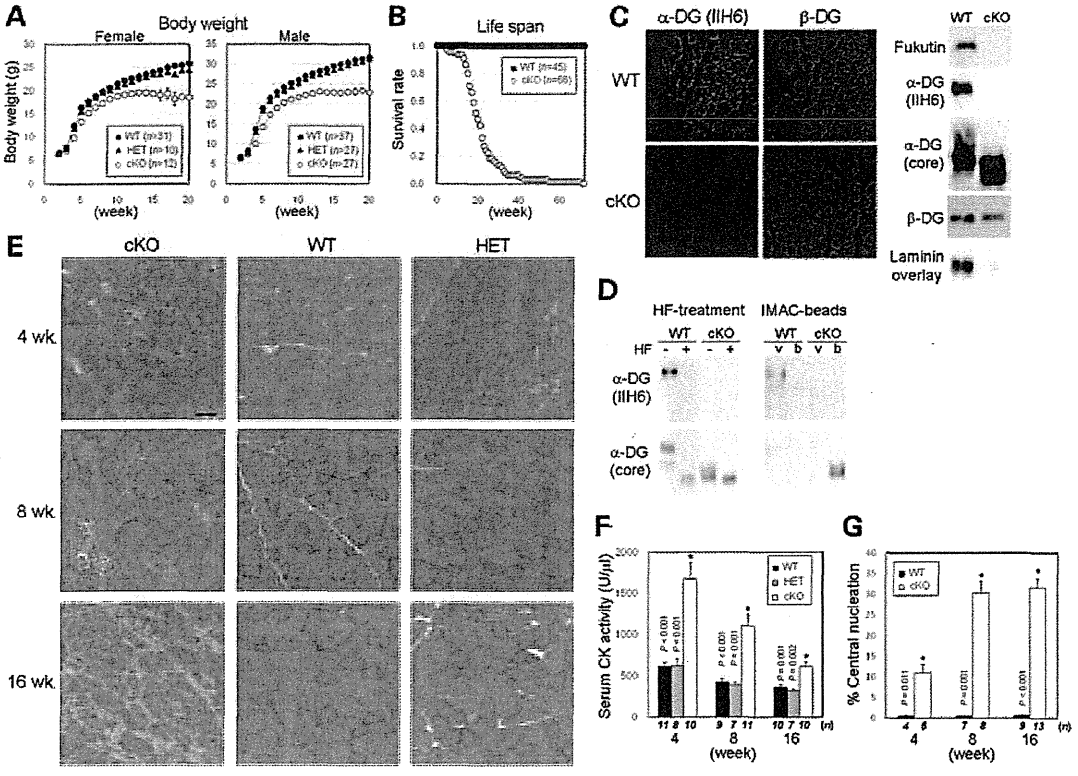

Figure 2. Pathological characterization of Myf5-fukutin-cKO mice. (**A**) Temporal changes in body weight. Data shown are mean ± SEM for each group (*n* is indicated in the graph). (**B**) Survival curve of Myf5-fukutin cKO mice. (**C**) Immunofluorescence and western blot analyses of fukutin expression and α-DG modification. Skeletal muscles of new born and 1-week-old Myf5-fukutin-cKO and control WT mice were used for immunofluorescence and western blotting, respectively. β-DG was used as a control. Laminin-binding activity of α-DG was examined by the laminin overlay assay. (**D**) Post-phosphoryl modification of α-DG from Myf5-fukutin-cKO and control WT skeletal muscles. The absence of post-phosphoryl modification was tested by HF treatment and IMAC-bead-binding assay. The void (v) and bound (b) fractions of the IMAC beads were analyzed by western blotting. (**E**) H&E staining of tibialis anterior muscles. Bar = 50 μm. (**F**) Serum creatin kinase activity and (**G**) proportion of myofibers with centrally located nuclei. Data shown are mean ± SEM for each group (*n* is indicated in the graph). $^*P \leq 0.05$ for both cKO versus WT and cKO versus HET (F) and cKO versus WT (G) (Mann–Whitney *U* test; *P*-values are indicated in the graph).

modification plays important roles in maintaining MPC viability, and consequently, muscle regeneration capability, suggesting that these defects may contribute to the severe phenotype of dystroglycanopathy.

Amelioration of the severe pathology by limited fukutin rescue in myofibers

Our pathological analysis of the two distinct fukutin-cKO mice suggested that membrane fragility triggers disease manifestation and that impaired MPC viability is related to disease progression and severity of dystroglycanopathy. These findings indicate that a therapeutic strategy must involve prevention of myofiber membrane weakness and/or rescue of substantial loss and dysfunction of MPCs. In addition, dystroglycanopathy is usually diagnosed after disease manifestation, and thus, treatments should be effective even after disease progression. Since our data suggested that frequent cycles of myofiber degeneration/regeneration accelerate substantial and/or functional loss of MPC, we expected that protection from disease-triggering myofiber degeneration provides therapeutic effects even in mouse models with MPC defects. In this study, to prevent disease-causing myofiber degeneration, we examined whether rescue of fukutin expression that is limited in myofibers is therapeutically beneficial in Myf5-fukutin-cKO mice. Therefore, we constructed recombinant AAV9 (AAV, adeno-associated virus) vectors containing the mouse *fukutin* cDNA under the MCK promoter (AAV9-MCK-*fukutin*).

We first administered intramuscular injections of AAV9-MCK-*fukutin* to 1-week-old (i.e. before disease manifestation) or 8-week-old (i.e. after disease manifestation) Myf5-fukutin-cKO mice; then, we examined the therapeutic effects after 2 months. In both cases, fukutin protein expression was higher in the AAV-injected Myf5-fukutin-cKO muscles than in the control WT muscles (endogenous fukutin protein in muscle lysates is below detectable levels) (Fig. 4A and E). IIH6-positive α-DG was restored, indicating functional rescue of *fukutin* gene expression even in adult cases (Fig. 4A, B, E and F). Histological and quantitative analyses showed that gene transfer at 1 week prevented disease manifestation (Fig. 4C and D). When gene transfer was challenged in 8-week-old mice, H&E staining showed milder phenotype in AAV-treated Myf5-fukutin-cKO muscles than

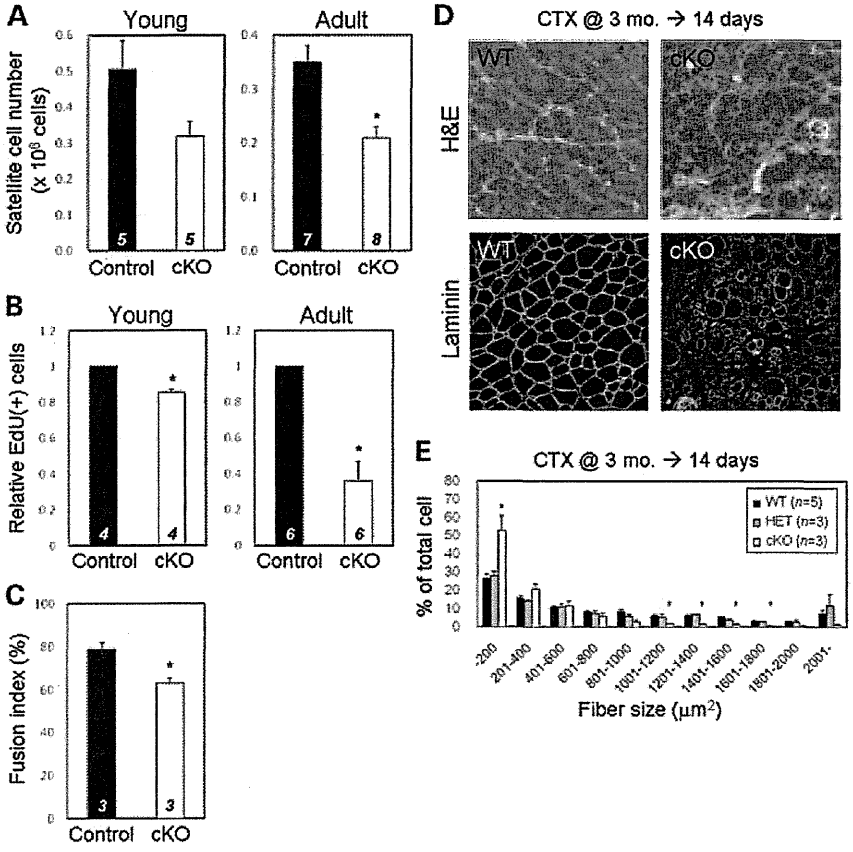

Figure 3. Impaired MPC activities and muscle regeneration in Myf5-fukutin-cKO mice. (**A**) The number of isolated satellite cells from young (2 weeks old) and adult (4 months old) Myf5-fukutin-cKO mice. $P = 0.117$ for young, and $P = 0.005$ for adult (Mann–Whitney U test). (**B**) Proliferation activity of the isolated MPCs. MPCs from young or adult Myf5-fukutin-cKO muscles were cultured for 2 days, and 5-ethynyl-2′-deoxyuridine-positive (EdU+) cells were counted. $P = 0.014$ for young, and $P = 0.002$ for adult (Mann–Whitney U test). (**C**) Differentiation activity of the isolated MPCs. MPCs from young Myf5-fukutin-cKO muscles were cultured in growth media for 2 days and then in differentiation media for 2 days. The cells were fixed, and multinucleated myotubes were counted. $P = 0.05$ (Mann–Whitney U test). For (A)–(C), data shown are mean ± SEM for each group (n is indicated in the graph). $^*P \leq 0.05$ compared with litter controls (Mann–Whitney U test). (**D**) Regeneration after CTX-induced muscle degeneration. CTX was injected into the tibialis anterior muscles of 3-month-old Myf5-fukutin-cKO and control mice (WT and HET). After 14 days, the muscle sections were analyzed by H&E staining and immunofluorescence staining with laminin. (**E**) Quantitative analysis for myofiber size variation after the CTX challenge. Data shown are mean ± SEM for each group (n is indicated in the graph). $^*P \leq 0.05$ for both cKO versus WT and cKO versus HET (Mann–Whitney U test).

in non-treated ones (Fig. 4G). Quantitatively, connective tissue infiltration and prevalence of small fibers were significantly reduced (Fig. 4H and I), whereas a substantial number of myofibers with central nucleation was still present after the gene transfer (Fig. 4J).

Next, we examined systemic delivery of the *fukutin* gene via tail vein injection into 4-week-old Myf5-fukutin-cKO mice with early-stage muscular dystrophy, primarily because diagnosis occurs during this stage in humans. After 2 months of the injection, we confirmed fukutin protein expression and recovery of α-DG modification in the treated Myf5-fukutin-cKO mice (Fig. 5A and B). After gene transfer, body and muscle weight were restored (Fig. 5C and D), and grip strength was dramatically improved, indicating recovery of muscle physiological function (Fig. 5E). H&E staining (Fig. 5F) and quantitative analyses of connective tissue infiltration (Fig. 5G) and fiber size variation (Fig. 5H) showed amelioration of muscle pathology; however, there were still a few necrotic fibers and a substantial proportion of myofibers with centrally located nuclei (Fig. 5I). Similar therapeutic effects were also obtained in other muscles (Supplementary Material, Fig. S4). Our results show that limited recovery of fukutin expression in myofibers, even after disease progression, can successfully ameliorate the severe phenotype of Myf5-fukutin-cKO mice.

We also constructed recombinant AAV9 vectors containing the mouse *fukutin* cDNA under the CMV promoter (AAV9-CMV-*fukutin*), which is commonly used for driving the expression of transgenes in a wide range of cell types. Two months after tail-vein injection in 4-week-old Myf5-fukutin-cKO mice, we observed therapeutic effects similar to those observed in AAV9-MCK-*fukutin*-treated Myf5-fukutin-cKO mice (Supplementary Material, Fig. S5). There was no obvious difference in the efficiency for the recovery of IIH6 immunoreactivity (the proportion of IIH6-positive to laminin-positive fibers) between the cases of AAV9-MCK-*fukutin* (77.4 ± 3.8%, $n = 5$) and AAV9-CMV-*fukutin* (74.8 ± 3.6%,

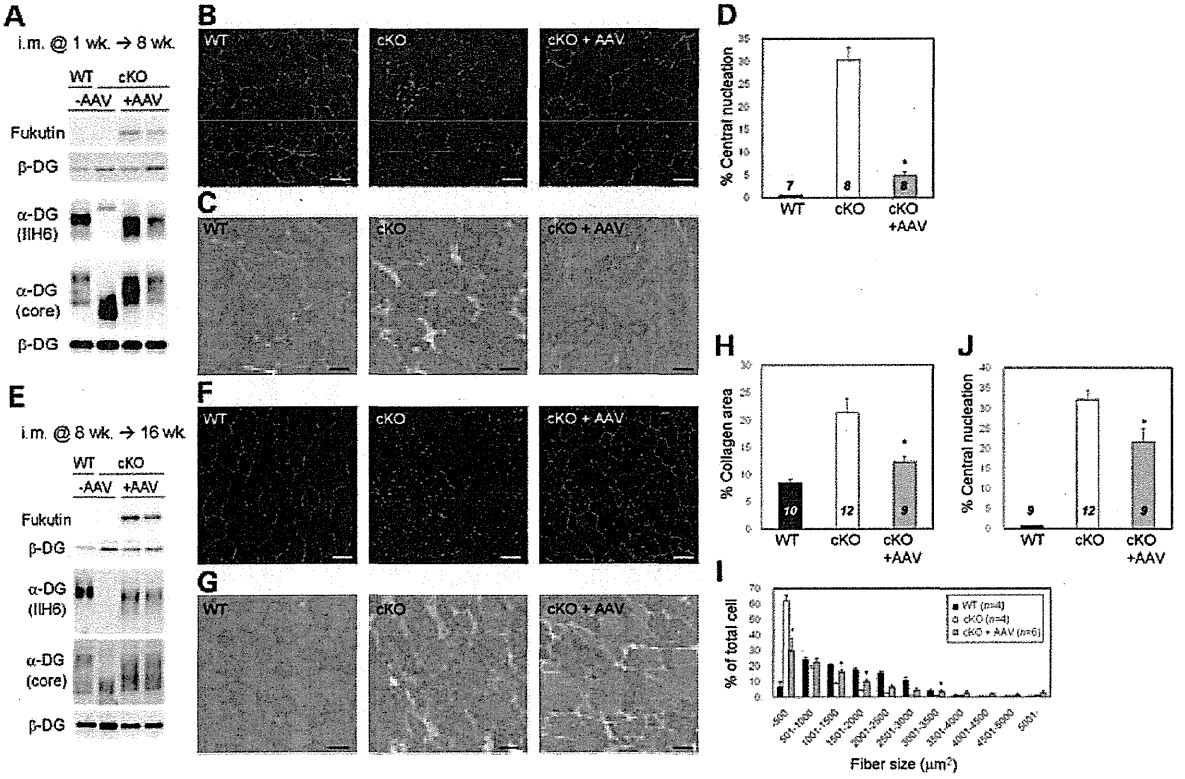

Figure 4. Gene transfer of *fukutin* via AAV9 intramuscular injection into Myf5-fukutin-cKO mice. AAV9-MCK-*fukutin* was administered to 1-week-old (**A**–**D**) and 8-week-old (**E**–**J**) Myf5-fukutin-cKO mice via intramuscular injection. Two months after the gene transfer, recovery of fukutin protein and α-DG glycosylation was confirmed by western blotting (A and E) and IIH6-immunofluorescence staining (B and F) (bar = 50 μm). For fukutin protein expression and α-DG modification, total lysate and wheat germ agglutinin-enriched fractions, respectively, were subjected to western blotting. In both cases, β-DG was used as a loading control. Western blotting results for two AAV-treated mice are shown. Therapeutic effects were quantitatively evaluated in terms of the proportion of myofibers with centrally located nuclei (D; $P = 0.001$, J; $P = 0.023$), connective tissue infiltration (H; $P = 0.016$) and fiber size variation (I; $^*P \leq 0.05$). Data shown are mean ± SEM for each group (n is indicated in the graph). $^*P \leq 0.05$ compared with non-treated cKO mice (Mann–Whitney U test).

$n = 5$). In addition, the population of myofibers with centrally located nuclei was significantly improved (Supplementary Material, Fig. S5I). We also examined the effects of intraperitoneal injections of AAV9-CMV-*fukutin* in 1-week-old Myf5-fukutin-cKO mice. Two months after the injections, we observed partial recovery of α-DG glycosylation and amelioration of the pathology compared with that observed in non-treated Myf5-fukutin-cKO mice (Supplementary Material, Fig. S6A–D).

The predominant mutation in FCMD is a retrotransposon insertion (4). We previously generated a transgenic knock-in mouse model carrying this insertion (29). The knock-in Hp/− mice represent compound heterozygotes for the insertion and a nonsense *fukutin* mutation. Although Hp/− mice show abnormal glycosylation of α-DG, a small amount of intact α-DG is also present; this prevents muscular dystrophy (29). We administered intraperitoneal injections of AAV9-CMV-*fukutin* to 1-week-old Hp/− mice and examined α-DG glycosylation status after 16 and 48 weeks. We detected increased levels of fukutin expression and IIH6-positive α-DG in the AAV-treated Hp/− skeletal muscles even 48 weeks after the gene transfer (Supplementary Material, Fig. S6E). These data suggest that the transferred *fukutin* gene persists in correcting abnormal glycosylation of α-DG for a considerable length of time.

DISCUSSION

In this study, we developed and analyzed two distinct *fukutin* cKO mice to understand the pathogenesis and to establish a therapeutic strategy for dystroglycanopathy. Our data showed that MPC-selective Myf5-fukutin-cKO mice exhibited more severe phenotypes of muscular dystrophy than myofiber-selective MCK-fukutin-cKO mice. Very recently, Campbell and colleagues also generated *fukutin* cKO mice, using Myf5-Cre and MCK-Cre mice (30). Pathological analysis of our Myf5-fukutin-cKO and MCK-fukutin-cKO mice showed results that were mostly consistent with those reported by Campbell and colleagues: increased serum CK levels in both cKO lines; milder phenotypes of MCK-fukutin-cKO than Myf5-fukutin-cKO; and decreases in grip strength, body mass and longevity of Myf5-fukutin-cKO mice. Our study includes further detailed histopathological characterization of the disease onset and progression in both lines. More importantly, our present study clarifies features of dystroglycanopathy that

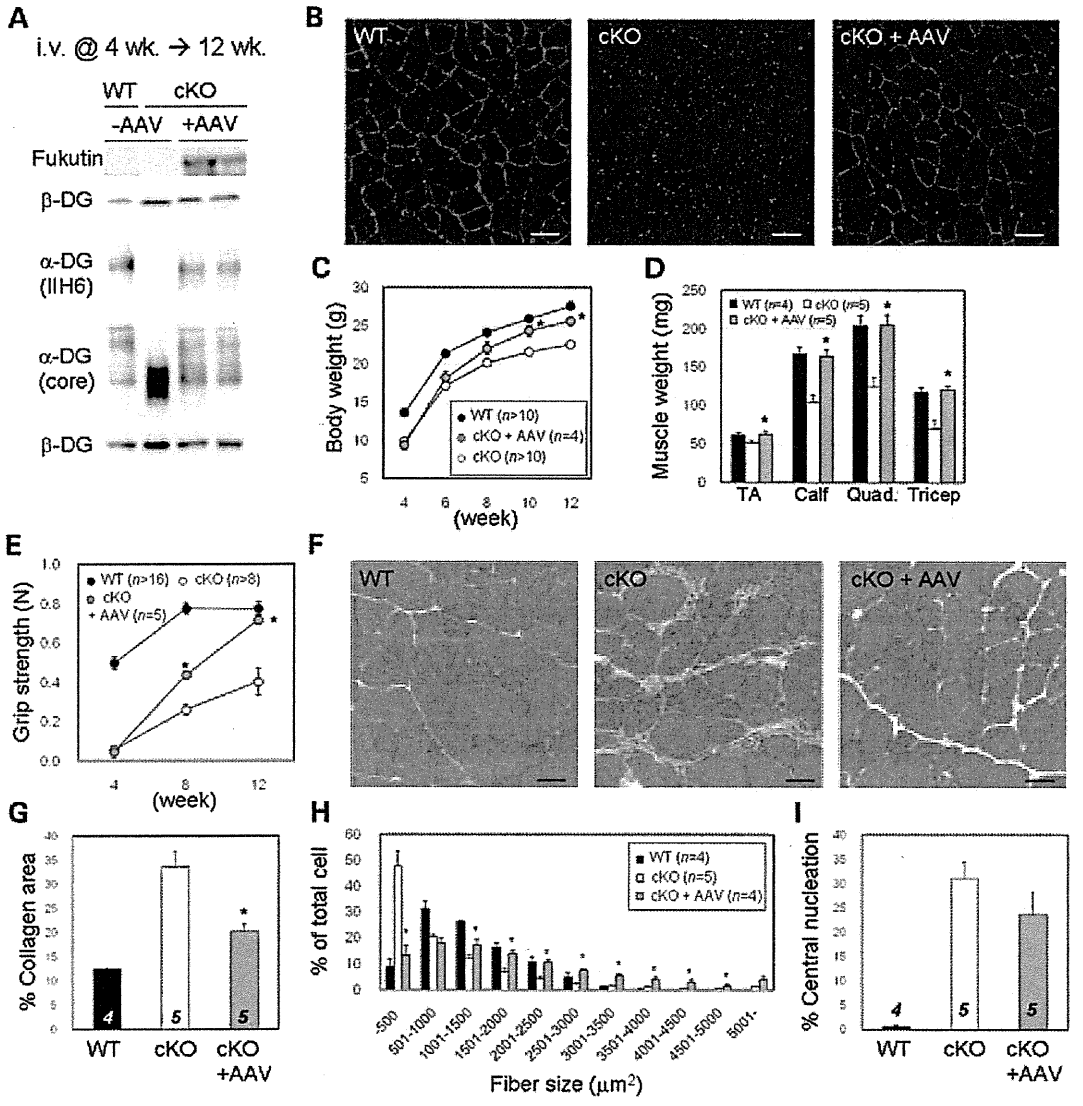

Figure 5. Systemic gene transfer of *fukutin* into Myf5-fukutin-cKO mice. AAV9-MCK-*fukutin* was administered to 4-week-old Myf5-fukutin-cKO mice via tail vein injection. Two months after the gene transfer, the skeletal muscles were analyzed and compared with non-treated Myf5-fukutin-cKO muscles. Recovery of fukutin protein and α-DG modification was confirmed by western blotting (**A**) and immunofluorescence (**B**) (bar = 50 μm). For fukutin protein expression and α-DG modification, total lysate and wheat germ agglutinin-enriched fractions, respectively, were subjected to western blotting. In both cases, β-DG was used as a loading control. Therapeutic effects were evaluated by body weight change (**C**; $P = 0.016$ and 0.01 for 10 and 12 weeks, respectively) and muscle weight change (**D**; $P = 0.047$ for tibialis anterior, and 0.014 for other muscles), grip strength (**E**; $P = 0.007$ and 0.003 for 8 and 12 weeks, respectively), H&E staining (**F**) (bar = 50 μm), connective tissue infiltration estimated by quantification of collagen I immunoreactive areas (**G**; $P = 0.028$), fiber size variation (**H**; $^*P \leq 0.05$) and central nucleation (**I**). Data from the tibialis anterior muscle are shown (F–I). Histopathology (F) and quantitative analyses (G and H) indicate amelioration of disease severity after the gene transfer. Data shown are mean ± SEM for each group (*n* is indicated in the graph). $^*P \leq 0.05$ compared with the non-treated cKO mice (Mann–Whitney *U* test). TA, tibialis anterior; Quad., quadricep.

enhance our understanding of its pathogenesis—specifically, the trigger initiating disease pathogenesis and the biological mechanism underlying the severe phenotype.

Our study provides direct evidence using presymptomatic fukutin-deficient mice that myofiber membrane fragility triggers disease manifestation. Although histological data in both studies suggested regeneration delay or impairment in Myf5-fukutin-cKO skeletal muscles, our study provides the first direct evidence for impaired MPC activity and viability using the isolated myoblast culture system. We observed that the proliferation and differentiation activities of the isolated MPCs from little-affected young Myf5-fukutin-cKO muscles were decreased, which may suggest that fukutin-dependent modification of α-DG plays a role in MPCs. Furthermore, our data showed that MPC proliferation and muscle regeneration deteriorate more severely as the disease progresses. The mechanisms underlying the decreases in the number of isolated satellite cells and MPC proliferation are

currently unknown. It has been suggested that satellite cells express properly glycosylated α-DG (31) and that myoblasts/MPCs also express properly glycosylated α-DG although its signals are relatively weak compared with those of myotubes (32,33). The basement membrane of skeletal muscle contains DG ligands, laminins and perlecan. It is well established that interactions between the extracellular matrix and cell-surface receptors are involved in cell survival signaling (34). Since it has been proposed that DG-ligand interactions are also involved in cellular signaling mechanisms such as survival and apoptosis pathways (35,36), it is possible that loss of α-DG glycosylation may affect survival signaling regulated by α-DG-basement membrane interaction. In addition, since the Myf5-fukutin-cKO myofibers showed an earlier reduction of fukutin compared with those of MCK-fukutin-cKO, there is a possibility that earlier loss of α-DG glycosylation in myofibers affects disease progression and severity. For example, the absence of α-DG glycosylation during postnatal/juvenile muscle growth and development may have a high impact on muscle degeneration and/or dystrophic pathology in later stages.

As for other muscular dystrophy models with defects in the dystrophin–glycoprotein complex, impaired muscle regeneration has also been reported in *MORE-DG null* mice, in which the DG gene (*Dag1*) is ablated in all cells in the embryo (31), and in older (>1 year) dystrophin-deficient mdx and sarcoglycan-deficient mice (31). The regeneration defects in our Myf5-fukutin-cKO mice appeared at a relatively young age (~3 months), but at this age, Myf5-fukutin-cKO mice already show severe dystrophic pathology. The pathological environment may interfere with efficient muscle regeneration, resulting in decreased regeneration activity as the disease progresses (37). A very recent study also suggested that alterations to the basal lamina microenvironment perturb regeneration potential in dystroglycanopathy (38). Moreover, our data suggest that multiple cycles of degeneration/regeneration may also affect MPC viability, which is consistent with a previous study showing that the progressive exhaustion of functional muscle satellite cells is associated with severe dystrophic phenotype (39). It appears that these disease environments and impaired MPC viability caused by loss of fukutin-dependent modification additively deteriorate regeneration activity, eventually leading to severe and rapid progressive pathology. Together, we conclude that defects in MPC activity contribute to the severe pathology of dystroglycanopathy and propose that dystroglycanopathy is a regeneration-defective disorder.

We observed that some muscle specimens from 16-week-old Myf5-fukutin-cKO mice showed mild phenotype, which was consequently supported by the presence of functionally glycosylated α-DG. Beedle *et al.* (30) also reported that fukutin deletion resulted in moderate to severe muscular dystrophy using Myf5-Cre mice. Because phenotypic variation in our Myf5-fukutin-cKO colony was rarely seen before 12 weeks of age, the variation may be secondary to disease progression. The less phenotypic variation in our colonies could also be due to the number of backcross on C57BL/6 (backcross: more than seven). We speculate that during frequent cycles of muscle degeneration/regeneration, Myf5-independent or less-expressed myogenic cells (40) may be activated and differentiated into myofibers in which the *fukutin* gene escaped Cre-mediated recombination.

Many cases of dystroglycanopathy show the most severe skeletal muscle phenotype, and the severe/typical dystroglycanopathy patients end their short lives without ever standing or walking. Although an increasing number of patients are being diagnosed with dystroglycanopathy worldwide, there have been no therapeutic studies on dystroglycanopathy models after the disease progresses. In this study, for the first time, we succeeded in ameliorating the disease severity in dystroglycanopathy mouse models based on the pathomechanism. It is of importance that limited rescue of fukutin protein in myofibers of Myf5-fukutin-cKO muscles, which have MPC defects, ameliorated the severe phenotype. These data suggest that even after functional and/or substantial loss of MPC occurs, prevention of disease-causing defects in myofibers is a probable therapeutic strategy for muscular dystrophy. Moreover, it is noteworthy that therapeutic effects of the exogenous *fukutin* gene were achieved with relatively lower AAV titers than those used in other gene therapies for structural proteins such as dystrophin and sarcoglycans (41–43). Our results showed that titers that were ~2 orders of magnitude less than those required in previous studies were sufficient to produce a therapeutic effect in Myf5-fukutin-cKO mice. This is consistent with our previous study, which suggested that only a little amount of fukutin is necessary to prevent muscular dystrophy (29). Most dystroglycanopathy genes are identified as glycosyltransferases (11,12,15) or hypothesized to have enzyme-like properties, suggesting that a small amount of exogenous gene would be sufficient for producing therapeutic effects. A small dose of AAV vectors could lower the chances of adverse effects such as immune responses in human (44). In addition, the cDNA sizes of fukutin as well as other dystroglycanopathy genes are suitable for AAV vectors. Taken together, we propose that gene transfer is a promising therapeutic strategy for the amelioration of the severe skeletal muscle pathology of dystroglycanopathy. Human dystroglycanopathy is frequently accompanied by brain and, often, cardiac disorders (1,45). The efficacy of AAV delivery to these affected tissues, timing of administration and therapeutic effects in other fukutin-cKO models should be examined in the future. Although therapeutic interventions that rescue the developmental defects of dystroglycanopathy (such as anomalies in brain structure) are difficult at present, amelioration of the muscle phenotype would be highly beneficial to patients and their families. For example, such treatment might improve patients' physical abilities and postpone the need for respiratory interventions until much later in the course of the disease. Increased physical activity could positively influence both mental development and social interactions. Overall, this study may facilitate future clinical translational research in the field of dystroglycanopathy treatment.

MATERIALS AND METHODS

Generation of fukutin cKO mice

Construction of the targeted allele, establishment of targeted embryonic stem (ES) cells and generation of the chimera

and F1 mice were carried out by Unitech Co. (Kashiwa, Japan). Briefly, exon 2 of mouse *fukutin* was flanked by two loxP sequences (Supplementary Material, Fig. S1A). An Flp recognition target-flanked neo-cassette was inserted upstream of exon 2. The targeting vector was electroporated into C57BL/6 mouse ES cells. Positive clones were selected, and homologous recombination was confirmed by Southern blotting (Supplementary Material, Fig. S1B). The targeted ES cells were injected into blastocysts (BALB/c), and then, chimera mice were bred with C57BL/6 mice to generate founder mice. The founder mice were crossed with the FLPe transgenic mice, producing heterozygous flox mice without the neo-cassette ($fukutin^{lox/+}$). The heterozygous flox mice were intercrossed to obtain homozygous flox mice ($fukutin^{lox/lox}$).

MCK-Cre mice (22) [$MCK\text{-}Cre^{Tg}(+)$, backcrossed for at least 10 generations to C57BL/6] and Myf5-Cre knock-in mice (23) [$Myf5\text{-}Cre^{KI}(+)$] were obtained from The Jackson Laboratory. Myf5-Cre mice were backcrossed for more than six generations to C57BL/6 before crossing with $fukutin^{lox/lox}$ mice. The heterozygous $fukutin^{lox/+}$ carrying MCK-Cre [$fukutin^{lox/+}$:$MCK\text{-}Cre^{Tg}(+)$] or Myf5-Cre [$fukutin^{lox/+}$:$Myf5\text{-}Cre^{KI}(+)$] were then bred with $fukutin^{lox/lox}$ mice to obtain cKO mice. Using this breeding strategy, we obtained the following four genotypes (Supplementary Material, Fig. S1C): for MCK-fukutin-cKO line—[$fukutin^{lox/lox}$:$MCK\text{-}Cre^{Tg}(-)$] (used as WT control), [$fukutin^{lox/lox}$:$MCK\text{-}Cre^{Tg}(+)$] (used as cKO), [$fukutin^{lox/+}$:$MCK\text{-}Cre^{Tg}(+)$] (used as heterozygous control, HET) and [$fukutin^{lox/+}$:$MCK\text{-}Cre^{Tg}(-)$]; and for the Myf5-fukutin-cKO line—[$fukutin^{lox/lox}$:$Myf5\text{-}Cre^{KI}(-)$] (used as WT), [$fukutin^{lox/lox}$:$Myf5\text{-}Cre^{KI}(+)$] (used as cKO), [$fukutin^{lox/+}$:$Myf5\text{-}Cre^{KI}(+)$] (used as HET) and [$fukutin^{lox/+}$:$Myf5\text{-}Cre^{KI}(-)$]. Alternatively, we crossed cKO mice with $fukutin^{lox/lox}$ mice to obtain two genotypes: WT and cKO (Supplementary Material, Fig. S1C). Genotyping was performed using PCR (Supplementary Material, Fig. S1D). Primer sequences and PCR conditions are available on request. Mice were maintained in accordance with the animal care guidelines of Unitech Co. Ltd., Osaka University and Kobe University.

Antibodies

Antibodies used in western blots and immunofluorescence were as follows: mouse monoclonal antibody 8D5 against β-DG (Novacastra); mouse monoclonal antibody IIH6 against glycosylated α-DG (Millipore); goat polyclonal antibody against the C-terminal domain of the α-DG polypeptide (AP-074G-C) (29); goat polyclonal anti-fukutin antibody (106G2) and rabbit polyclonal anti-fukutin antibody (RY213) (5); rat anti-laminin antibody 4H8-2 (Alexis Biochemicals); rabbit polyclonal anti-collagen I antibody (AbD Serotec); and mouse monoclonal anti-embryonic myosin antibody (The Developmental Studies Hybridoma Bank, University of Iowa). A rat monoclonal antibody against the α-DG core protein (3D7-7) was generated using the recombinant α-DG-Fc fusion protein (46); hybridoma clones were selected for reactivity to the C-terminal domain of the α-DG polypeptide. To reduce high background staining of IIH6 in severely affected skeletal muscle sections, commercial IIH6 was labeled with biotin. The IIH6-IgM fractions were prepared from ascites, using protein L-beads (Pierce) and then biotinylated (EZ-Link Micro Sulfo-NHS-Biotinylation Kit; Pierce) according to the manufacturer's instructions.

Preparation of fukutin and DG

Endogenous fukutin was enriched by immunoprecipitation using polyclonal goat anti-fukutin antibody (106G2) from the skeletal muscle lysates. The immunoprecipitated materials were subjected to western blotting using polyclonal rabbit anti-fukutin antibody (RY213). DG from solubilized skeletal muscle was enriched with wheat germ agglutinin-agarose beads (Vector Laboratories) as previously described (29).

Histological and immunofluorescence analyses

For histological and immunofluorescence staining, cryosections (7 μm thick) were prepared. For H&E staining, sections were stained for 2 min in hematoxylin, 1 min in eosin, and then dehydrated with ethanol and xylene. The slides are washed with 0.5% glacial acetic acid, dehydrated and then mounted. For immunofluorescence analysis, sections were treated with cold ethanol/acetic acid (1:1) for 1 min, blocked with 5% goat serum in MOM mouse Ig blocking reagent (Vector Laboratories) at room temperature for 1 h, and then incubated overnight with primary antibodies diluted in MOM diluent (Vector Laboratories) at 4°C. The slides were washed with phosphate-buffered saline (PBS) and incubated with Alexa Fluor 488-conjugated or Alexa Fluor 555-conjugated secondary antibodies (Molecular Probes) at room temperature for 30 min. Sections were observed by fluorescence microscopy (Leica DMR, Leica Microsystems and BZ9000, Keyence). Quantification of the number of Pax7-positive cells and the population of Pax7/MyoD-double-positive cells was performed as previously described (47).

Quantitative and statistical analysis

For quantitative evaluation of muscle pathology, the proportion of myofibers with centrally located nuclei in at least 1000 fibers for each individual was counted. For the evaluation of connective tissue infiltration, the immunofluorescence signal of collagen I was quantitatively measured using the ImageJ software. For the assessment of myofiber size variation, areas of individual myofibers on transverse sections were measured using the ImageJ software. Data represent means with SEM, and P-values ≤ 0.05 were considered statistically significant (Mann–Whitney U test).

Preparation and culture of MPCs

Mononuclear cells from uninjured limb muscles were prepared using 0.2% collagenase type II (Worthington Biochemical) as previously described (28,48). Approximately $3-5 \times 10^6$ or $3-9 \times 10^6$ mononuclear cells from young mice (2-week-old) or adult mice (4-month-old), respectively, were subjected to MPC isolation experiments. Mononuclear cells derived from the skeletal muscles were stained with FITC-conjugated anti-CD31 (Pecam1, Mouse Genome Informatics), anti-CD45

(Ptprc, Mouse Genome Informatics), phycoerythrin-conjugated anti-Sca1 (Ly6a, Mouse Genome Informatics) and biotinylated SM/C-2.6 antibodies (28). Cells were then incubated with 1:400 streptavidin–allophycocyanin (BD Biosciences) on ice for 30 min and resuspended in PBS containing 2% fetal calf serum (FCS) and 2 μg/ml propidium iodide (PI). Cell sorting was performed using an FACS Aria II flow cytometer (BD Immunocytometry Systems). Debris and dead cells were excluded by forward scatter, side scatter and PI gating. Data were collected using the FACSDiva software (BD Biosciences). Myogenic cells from the regenerating muscles were also highly enriched in the SM/C-2.6(+) CD31(−) CD45(−) Sca1(−) cell fraction.

Freshly isolated myogenic cells were cultured in a growth medium of high-glucose Dulbecco's modified Eagle's medium (DMEM-HG; Sigma-Aldrich) containing 20% FCS, 2.5 ng/ml basic fibroblast growth factor (FGF2; PeproTech) and penicillin (100 U/ml)–streptomycin (100 μg/ml) (Gibco BRL) on culture dishes coated with Matrigel (BD Biosciences). Differentiation was induced in a differentiation medium containing DMEM-HG, 5% horse serum and penicillin–streptomycin for 3–4 days. Quantitative analysis for cell proliferation was performed as described previously (47). Fusion index was estimated as the ratio of nuclei in the myotubes to all the nuclei in more than four independent microscopy fields.

CTX experiments

CTX (30 μM; purified from the venom of the snake *Naja nigricollis*; Latoxan) was injected intramuscularly (for young mice, 30 μl to the tibialis anterior and 70 μl to the calf; for adult mice, 50 μl to the tibialis anterior and 100 μl to the calf). Mock injections used only saline solution. The injected muscles were examined 5 or 14 days after the injection. Five days after the injection, areas of individual embryonic myosin-positive fibers were measured (>300 fibers randomly chosen from 5–10 regions per toxin-challenged muscle) in each genotype. Fourteen days after the injection, fiber size variation was quantitatively evaluated by measuring individual laminin-positive fibers (>300 fibers) in each genotype.

AAV gene transfer

To generate *fukutin*-encoding AAV9 vector, the complete open reading frame of mouse *fukutin* gene was cloned into the pAAV-IRES-hrGFP vector (49). The recombinant *fukutin*-encoding AAV9 vector was produced as described previously (49). AAV vectors were injected intramuscularly into the calf and tibialis anterior (at 1 week to the tibialis anterior, $0.8–1.6 \times 10^9$ vector genome in saline solution; at 1 week to the calf or at 8 weeks to the tibialis anterior, $2–4 \times 10^9$ vector genome; and at 8 weeks to the calf, $4–8 \times 10^9$ vector genome). For tail vein injections and intraperitoneal injections, $\sim 2 \times 10^{10}$ and $\sim 1 \times 10^{10}$ vector genome was used, respectively.

Miscellaneous

For western blotting, the proteins were separated using 4–15% linear gradient SDS–PAGE (Bio-Rad). Gels were transferred to polyvinylidene fluoride membrane (Millipore). Blots were developed by horseradish peroxidase-enhanced chemiluminescence (Supersignal West Pico, Pierce; or ECL Plus, GE Healthcare). Laminin-binding activity was determined by the laminin overlay assay as described previously (29). Serum CK activity was measured using the CPK kit (WAKO). For Evans blue dye uptake, Evans blue dye (10 mg/ml in saline) was intraperitoneally injected (100 μl/10 g of body weight). After 5 h, the mice were made to exercise on a downhill (15°) treadmill for 60 min (MK-680S, Muromachi Kikai). Twenty-four hours after the exercise, frozen tissue samples were prepared. Serum was prepared before 24 h and after 2 h of the exercise. Grip strength was measured for 10 consecutive trials for each mouse, using a strength meter (Ohara Ika Sangyo Co. Ltd, Tokyo), and 20% of the top and the bottom values were excluded to obtain the mean value.

SUPPLEMENTARY MATERIAL

Supplementary Material is available at *HMG* online.

ACKNOWLEDGEMENTS

We would like to thank the past and present members of T.T.'s laboratory for fruitful discussions and scientific contributions. We also thank Hiromi Hayashita-Kinoh for providing technical support.

Conflict of Interest statement. None declared.

FUNDING

This work was supported by the Ministry of Health, Labor and Welfare of Japan [Intramural Research Grant for Neurological and Psychiatric Disorders of National Center of Neurology and Psychiatry (23B-5)], the Ministry of Education, Culture, Sports, Science and Technology of Japan [a Grant-in-Aid for Scientific Research (A) 23249049 to T.T., a Grant-in-Aid for Young Scientists (A) 24687017 to M.K. and a Grant-in-Aid for Scientific Research on Innovative Areas (No. 23110002, Deciphering Sugar Chain-based Signals Regulating Integrative Neuronal Functions) 24110508 to M.K.], a Senri Life Science Foundation grant to M.K., a Takeda Science Foundation grant to M.K. and a Naito Foundation grant to M.K.

REFERENCES

1. Godfrey, C., Foley, A.R., Clement, E. and Muntoni, F. (2011) Dystroglycanopathies: coming into focus. *Curr. Opin. Genet. Dev.*, **21**, 278–285.
2. Hayashi, Y.K., Ogawa, M., Tagawa, K., Noguchi, S., Ishihara, T., Nonaka, I. and Arahata, K. (2001) Selective deficiency of alpha-dystroglycan in Fukuyama-type congenital muscular dystrophy. *Neurology*, **57**, 115–121.
3. Michele, D.E., Barresi, R., Kanagawa, M., Saito, F., Cohn, R.D., Satz, J.S., Dollar, J., Nishino, I., Kelley, R.I., Somer, H. *et al.* (2002) Post-translational disruption of dystroglycan-ligand interactions in congenital muscular dystrophies. *Nature*, **418**, 417–422.
4. Kobayashi, K., Nakahori, Y., Miyake, M., Matsumura, K., Kondo-Iida, E., Nomura, Y., Segawa, M., Yoshioka, M., Saito, K., Osawa, M. *et al.* (1998) An ancient retrotransposal insertion causes Fukuyama-type congenital muscular dystrophy. *Nature*, **394**, 388–392.

5. Taniguchi-Ikeda, M., Kobayashi, K., Kanagawa, M., Yu, C.C., Mori, K., Oda, T., Kuga, A., Kurahashi, H., Akman, H.O., DiMauro, S. *et al.* (2011) Pathogenic exon-trapping by SVA retrotransposon and rescue in Fukuyama muscular dystrophy. *Nature*, **478**, 127–131.
6. Fukuyama, Y., Osawa, M. and Suzuki, H. (1981) Congenital progressive muscular dystrophy of the Fukuyama type-clinical, genetic and pathological considerations. *Brain Dev.*, **3**, 1–29.
7. Godfrey, C., Clement, E., Mein, R., Brockington, M., Smith, J., Talim, B., Straub, V., Robb, S., Quinlivan, R., Feng, L. *et al.* (2007) Refining genotype phenotype correlations in muscular dystrophies with defective glycosylation of dystroglycan. *Brain*, **130**, 2725–2735.
8. Tachikawa, M., Kanagawa, M., Yu, C.C., Kobayashi, K. and Toda, T. (2012) Mislocalization of fukutin protein by disease-causing missense mutations can be rescued with treatments directed at folding amelioration. *J. Biol. Chem.*, **287**, 8398–8406.
9. Wells, L. (2013) The O-mannosylation pathway: glycosyltransferases and proteins implicated in congenital muscular dystrophy. *J. Biol. Chem.*, **288**, 6930–6935.
10. Buysse, K., Riemersma, M., Powell, G., van Reeuwijk, J., Chitayat, D., Roscioli, T., Kamsteeg, E.J., van den Elzen, C., van Beusekom, E., Blaser, S. *et al.* (2013) Missense mutations in β-1,3-*N*-acetylglucosaminyltransferase 1 (B3GNT1) cause Walker-Warburg syndrome. *Hum. Mol. Genet.*, **22**, 1746–1754.
11. Manya, H., Chiba, A., Yoshida, A., Wang, X., Chiba, Y., Jigami, Y., Margolis, R.U. and Endo, T. (2004) Demonstration of mammalian protein *O*-mannosyltransferase activity: coexpression of POMT1 and POMT2 required for enzymatic activity. *Proc. Natl Acad. Sci. USA*, **101**, 500–505.
12. Yoshida, A., Kobayashi, K., Manya, H., Taniguchi, K., Kano, H., Mizuno, M., Inazu, T., Mitsuhashi, H., Takahashi, S., Takeuchi, M. *et al.* (2001) Muscular dystrophy and neuronal migration disorder caused by mutations in a glycosyltransferase, POMGnT1. *Dev. Cell*, **1**, 717–724.
13. Yoshida-Moriguchi, T., Yu, L., Stalnaker, S.H., Davis, S., Kunz, S., Madson, M., Oldstone, M.B., Schachter, H., Wells, L. and Campbell, K.P. (2010) *O*-mannosyl phosphorylation of alpha-dystroglycan is required for laminin binding. *Science*, **327**, 88–92.
14. Kuga, A., Kanagawa, M., Sudo, A., Chan, Y.M., Tajiri, M., Manya, H., Kikkawa, Y., Nomizu, M., Kobayashi, K., Endo, T. *et al.* (2012) Absence of post-phosphoryl modification in dystroglycanopathy mouse models and wild-type tissues expressing non-laminin binding form of α-dystroglycan. *J. Biol. Chem.*, **287**, 9560–9567.
15. Inamori, K., Yoshida-Moriguchi, T., Hara, Y., Anderson, M.E., Yu, L. and Campbell, K.P. (2012) Dystroglycan function requires xylosyl- and glucuronyltransferase activities of LARGE. *Science*, **335**, 93–96.
16. Ibraghimov-Beskrovnaya, O., Ervasti, J.M., Leveille, C.J., Slaughter, C.A., Sernett, S.W. and Campbell, K.P. (1992) Primary structure of dystrophin-associated glycoproteins linking dystrophin to the extracellular matrix. *Nature*, **355**, 696–702.
17. Barresi, R. and Campbell, K.P. (2006) Dystroglycan: from biosynthesis to pathogenesis of human disease. *J. Cell Sci.*, **119**, 199–207.
18. Taniguchi, M., Kurahashi, H., Noguchi, S., Fukudome, T., Okinaga, T., Tsukahara, T., Tajima, Y., Ozono, K., Nishino, I., Nonaka, I. and Toda, T. (2006) Aberrant neuromuscular junctions and delayed terminal muscle fiber maturation in alpha-dystroglycanopathies. *Hum. Mol. Genet.*, **15**, 1279–1289.
19. Hara, Y., Balci-Hayta, B., Yoshida-Moriguchi, T., Kanagawa, M., Beltrán-Valero de Bernabé, D., Gündeşli, H., Willer, T., Satz, J.S., Crawford, R.W., Burden, S.J. *et al.* (2011) A dystroglycan mutation associated with limb-girdle muscular dystrophy. *N. Engl. J. Med.*, **364**, 939–946.
20. Roscioli, T., Kamsteeg, E.J., Buysse, K., Maystadt, I., van Reeuwijk, J., van den Elzen, C., van Beusekom, E., Riemersma, M., Pfundt, R., Vissers, L.E. *et al.* (2012) Mutations in ISPD cause Walker-Warburg syndrome and defective glycosylation of α-dystroglycan. *Nat. Genet.*, **44**, 581–585.
21. Willer, T., Lee, H., Lommel, M., Yoshida-Moriguchi, T., de Bernabe, D.B., Venzke, D., Cirak, S., Schachter, H., Vajsar, J., Voit, T. *et al.* (2012) ISPD loss-of-function mutations disrupt dystroglycan O-mannosylation and cause Walker-Warburg syndrome. *Nat. Genet.*, **44**, 575–580.
22. Brüning, J.C., Michael, M.D., Winnay, J.N., Hayashi, T., Hörsch, D., Accili, D., Goodyear, L.J. and Kahn, C.R. (1998) A muscle-specific insulin receptor knockout exhibits features of the metabolic syndrome of NIDDM without altering glucose tolerance. *Mol. Cell*, **2**, 559–569.
23. Tallquist, M.D., Weismann, K.E., Hellström, M. and Soriano, P. (2000) Early myotome specification regulates PDGFA expression and axial skeleton development. *Development*, **127**, 5059–5070.
24. Lyons, G.E., Mühlebach, S., Moser, A., Masood, R., Paterson, B.M., Buckingham, M.E. and Perriard, J.C. (1991) Developmental regulation of creatine kinase gene expression by myogenic factors in embryonic mouse and chick skeletal muscle. *Development*, **113**, 1017–1029.
25. Trask, R.V. and Billadello, J.J. (1990) Tissue-specific distribution and developmental regulation of M and B creatine kinase mRNAs. *Biochim. Biophys. Acta*, **1049**, 182–188.
26. Vilquin, J.T., Brussee, V., Asselin, I., Kinoshita, I., Gingras, M. and Tremblay, J.P. (1998) Evidence of mdx mouse skeletal muscle fragility in vivo by eccentric running exercise. *Muscle Nerve*, **21**, 567–576.
27. Durbeej, M., Sawatzki, S.M., Barresi, R., Schmainda, K.M., Allamand, V., Michele, D.E. and Campbell, K.P. (2003) Gene transfer establishes primacy of striated vs. smooth muscle sarcoglycan complex in limb-girdle muscular dystrophy. *Proc. Natl Acad. Sci. USA*, **100**, 8910–8915.
28. Fukada, S., Higuchi, S., Segawa, M., Koda, K., Yamamoto, Y., Tsujikawa, K., Kohama, Y., Uezumi, A., Imamura, M., Miyagoe-Suzuki, Y. *et al.* (2004) Purification and cell-surface marker characterization of quiescent satellite cells from murine skeletal muscle by a novel monoclonal antibody. *Exp. Cell Res.*, **296**, 245–255.
29. Kanagawa, M., Nishimoto, A., Chiyonobu, T., Takeda, S., Miyagoe-Suzuki, Y., Wang, F., Fujikake, N., Taniguchi, M., Lu, Z., Tachikawa, M. *et al.* (2009) Residual laminin-binding activity and enhanced dystroglycan glycosylation by LARGE in novel model mice to dystroglycanopathy. *Hum. Mol. Genet.*, **18**, 621–631.
30. Beedle, A.M., Turner, A.J., Saito, Y., Lueck, J.D., Foltz, S.J., Fortunato, M.J., Nienaber, P.M. and Campbell, K.P. (2012) Mouse fukutin deletion impairs dystroglycan processing and recapitulates muscular dystrophy. *J. Clin. Invest.*, **122**, 3330–3342.
31. Cohn, R.D., Henry, M.D., Michele, D.E., Barresi, R., Saito, F., Moore, S.A., Flanagan, J.D., Skwarchuk, M.W., Robbins, M.E., Mendell, J.R., Williamson, R.A. and Campbell, K.P. (2002) Disruption of DAG1 in differentiated skeletal muscle reveals a role for dystroglycan in muscle regeneration. *Cell*, **110**, 639–648.
32. Barresi, R., Michele, D.E., Kanagawa, M., Harper, H.A., Dovico, S.A., Satz, J.S., Moore, S.A., Zhang, W., Schachter, H., Dumanski, J.P. *et al.* (2004) LARGE can functionally bypass alpha-dystroglycan glycosylation defects in distinct congenital muscular dystrophies. *Nat. Med.*, **10**, 696–703.
33. Hara, Y., Kanagawa, M., Kunz, S., Yoshida-Moriguchi, T., Satz, J.S., Kobayashi, Y.M., Zhu, Z., Burden, S.J., Oldstone, M.B. and Campbell, K.P. (2011) Like-acetylglucosaminyltransferase (LARGE)-dependent modification of dystroglycan at Thr-317/319 is required for laminin binding and arenavirus infection. *Proc. Natl Acad. Sci. USA*, **108**, 17426–17431.
34. Gilmore, A.P. (2005) Anoikis. *Cell Death Differ.*, **12**, 1473–1477.
35. Langenbach, K.J. and Rando, T.A. (2002) Inhibition of dystroglycan binding to laminin disrupts the PI3K/AKT pathway and survival signaling in muscle cells. *Muscle Nerve*, **26**, 644–653.
36. Munoz, J., Zhou, Y. and Jarrett, H.W. (2010) LG4-5 domains of laminin-211 binds alpha-dystroglycan to allow myotube attachment and prevent anoikis. *J. Cell. Physiol.*, **222**, 111–119.
37. Morgan, J.E. and Zammit, P.S. (2010) Direct effects of the pathogenic mutation on satellite cell function in muscular dystrophy. *Exp. Cell Res.*, **316**, 3100–3108.
38. Ross, J., Benn, A., Jonuschies, J., Boldrin, L., Muntoni, F., Hewitt, J.E., Brown, S.C. and Morgan, J.E. (2012) Defects in glycosylation impair satellite stem cell function and niche composition in the muscles of the dystrophic Large(myd) mouse. *Stem Cells*, doi: 10.1002/stem.1197.
39. Sacco, A., Mourkioti, F., Tran, R., Choi, J., Llewellyn, M., Kraft, P., Shkreli, M., Delp, S., Pomerantz, J.H., Artandi, S.E. and Blau, H.M. (2010) Short telomeres and stem cell exhaustion model Duchenne muscular dystrophy in mdx/mTR mice. *Cell*, **143**, 1059–1071.
40. Gensch, N., Borchardt, T., Schneider, A., Riethmacher, D. and Braun, T. (2008) Different autonomous myogenic cell populations revealed by ablation of Myf5-expressing cells during mouse embryogenesis. *Development*, **135**, 1597–1604.
41. Gregorevic, P., Allen, J.M., Minami, E., Blankinship, M.J., Haraguchi, M., Meuse, L., Finn, E., Adams, M.E., Froehner, S.C., Murry, C.E. and Chamberlain, J.S. (2006) rAAV6-Microdystrophin preserves muscle

function and extends lifespan in severely dystrophic mice. *Nat. Med.*, **12**, 787–789.
42. Yoshimura, M., Sakamoto, M., Ikemoto, M., Mochizuki, Y., Yuasa, K., Miyagoe-Suzuki, Y. and Takeda, S. (2004) AAV vector-mediated microdystrophin expression in a relatively small percentage of mdx myofibers improved the mdx phenotype. *Mol. Ther.*, **10**, 821–828.
43. Pacak, C.A., Walter, G.A., Gaidosh, G., Bryant, N., Lewis, M.A., Germain, S., Mah, C.S., Campbell, K.P. and Byrne, B.J. (2007) Long-term skeletal muscle protection after gene transfer in a mouse model of LGMD-2D. *Mol. Ther.*, **15**, 1775–1781.
44. Nathwani, A.C., Tuddenham, E.G., Rangarajan, S., Rosales, C., McIntosh, J., Linch, D.C., Chowdary, P., Riddell, A., Pie, A.J., Harrington, C. *et al.* (2011) Adenovirus-associated virus vector-mediated gene transfer in hemophilia B. *N. Engl. J. Med.*, **365**, 2357–2365.
45. Pane, M., Messina, S., Vasco, G., Foley, A.R., Morandi, L., Pegoraro, E., Mongini, T., D'Amico, A., Bianco, F., Lombardo, M.E. *et al.* (2012) Respiratory and cardiac function in congenital muscular dystrophies with alpha dystroglycan deficiency. *Neuromuscul. Disord.*, **22**, 685–689.
46. Kanagawa, M., Omori, Y., Sato, S., Kobayashi, K., Miyagoe-Suzuki, Y., Takeda, S., Endo, T., Furukawa, T. and Toda, T. (2010) Post-translational maturation of dystroglycan is necessary for pikachurin binding and ribbon synaptic localization. *J. Biol. Chem.*, **285**, 31208–31216.
47. Fukada, S., Yamaguchi, M., Kokubo, H., Ogawa, R., Uezumi, A., Yoneda, T., Matev, M.M., Motohashi, N., Ito, T., Zolkiewska, A. *et al.* (2011) Hesr1 and Hesr3 are essential to generate undifferentiated quiescent satellite cells and to maintain satellite cell numbers. *Development*, **138**, 4609–4619.
48. Segawa, M., Fukada, S., Yamamoto, Y., Yahagi, H., Kanematsu, M., Sato, M., Ito, T., Uezumi, A., Hayashi, S., Miyagoe-Suzuki, Y. *et al.* (2008) Suppression of macrophage functions impairs skeletal muscle regeneration with severe fibrosis. *Exp. Cell Res.*, **314**, 3232–3244.
49. Shin, J.H., Nitahara-Kasahara, Y., Hayashita-Kinoh, H., Ohshima-Hosoyama, S., Kinoshita, K., Chiyo, T., Okada, H., Okada, T. and Takeda, S. (2011) Improvement of cardiac fibrosis in dystrophic mice by rAAV9-mediated microdystrophin transduction. *Gene Ther.*, **18**, 910–919.

Parkinsonism and Related Disorders 19 (2013) 15–20

Contents lists available at SciVerse ScienceDirect

Parkinsonism and Related Disorders

journal homepage: www.elsevier.com/locate/parkreldis

Analyses of the *MAPT*, *PGRN*, and *C9orf72* mutations in Japanese patients with FTLD, PSP, and CBS

Kotaro Ogaki [a], Yuanzhe Li [b], Masashi Takanashi [a], Kei-Ichi Ishikawa [a], Tomonori Kobayashi [d], Takashi Nonaka [e], Masato Hasegawa [e], Masahiko Kishi [f], Hiroyo Yoshino [b], Manabu Funayama [a,b], Tetsuro Tsukamoto [g], Keiichi Shioya [h], Masayuki Yokochi [i], Hisamasa Imai [a], Ryogen Sasaki [j], Yasumasa Kokubo [j], Shigeki Kuzuhara [k], Yumiko Motoi [a], Hiroyuki Tomiyama [a,c], Nobutaka Hattori [a,b,c,*]

[a] *Department of Neurology, Juntendo University School of Medicine, Tokyo, Japan*
[b] *Research Institute for Diseases of Old Age, Juntendo University School of Medicine, Tokyo, Japan*
[c] *Department of Neuroscience for Neurodegenerative Disorders, Juntendo University School of Medicine, Tokyo, Japan*
[d] *Department of Neurology, Fukuoka University School of Medicine, Fukuoka, Japan*
[e] *Department of Neuropathology and Cell Biology, Tokyo Metropolitan Institute of Medical Science, Tokyo, Japan*
[f] *Department of Internal Medicine, Division of Neurology, Sakura Medical Center, Toho University, Sakura, Japan*
[g] *Department of Neurology, Numazu Rehabilitation Hospital, Numazu, Japan*
[h] *Department of Neurology, National Hospital Organization Miyazaki Higashi Hospital, Miyazaki, Japan*
[i] *Department of Neurology, Tokyo Metropolitan Health and Medical Treatment Corp., Ebara Hospital, Tokyo, Japan*
[j] *Department of Neurology, Mie University Graduate School of Medicine, Tsu, Mie, Japan*
[k] *Department of Medical Welfare, Faculty of Health Science, Suzuka University of Medical Science, Suzuka, Mie, Japan*

ARTICLE INFO

Article history:
Received 26 April 2012
Received in revised form
16 June 2012
Accepted 19 June 2012

Keywords:
MAPT
PGRN
C9orf72
De novo
Abnormal eye movements

ABSTRACT

Background: Mutations in the microtubule associated protein tau (*MAPT*) and progranulin (*PGRN*) have been identified in several neurodegenerative disorders, such as frontotemporal lobar degeneration (FTLD), progressive supranuclear palsy (PSP), and corticobasal syndrome (CBS). Recently, *C9orf72* repeat expansion was reported to cause FTLD and amyotrophic lateral sclerosis (ALS). To date, no comprehensive analyses of mutations in these three genes have been performed in Asian populations. The aim of this study was to investigate the genetic and clinical features of Japanese patients with *MAPT*, *PGRN*, or *C9orf72* mutations.

Methods: *MAPT* and *PGRN* were analyzed by direct sequencing and gene dosage assays, and *C9orf72* repeat expansion was analyzed by repeat-primed PCR in 75 (48 familial, 27 sporadic) Japanese patients with FTLD, PSP, or CBS.

Results: We found four *MAPT* mutations in six families, one novel *PGRN* deletion/insertion, and no repeat expansion in *C9orf72*. Intriguingly, we identified a *de novo MAPT* p.S285R mutation. All six patients with early-onset PSP and the abnormal eye movements that are not typical of sporadic PSP had *MAPT* mutations. The gene dosages of *MAPT* and *PGRN* were normal.

Discussion: *MAPT* p.S285R is the first reported *de novo* mutation in a sporadic adult-onset patient. *MAPT* mutation analysis is recommended in both familial and sporadic patients, especially in early-onset PSP patients with these abnormal eye movements. Although *PGRN* and *C9orf72* mutations were rare in this study, the *PGRN* mutation was found in this Asian FTLD. These genes should be studied further to improve the clinicogenetic diagnoses of FTLD, PSP, and CBS.

1. Introduction

Mutations in the microtubule-associated protein tau (*MAPT*) and the progranulin (*PGRN*) genes have been identified in families with frontotemporal dementia and parkinsonism linked to chromosome 17 [1–3]. Recently, two studies reported that the expansion of a noncoding GGGGCC hexanucleotide repeat in the *C9orf72* gene is

* Corresponding author. Department of Neurology, Juntendo University School of Medicine, 2-1-1 Hongo, Bunkyo, Tokyo 113-8421, Japan. Tel.: +81 3 5802 1073; fax: +81 3 5800 0547.
E-mail address: nhattori@juntendo.ac.jp (N. Hattori).

1353-8020/$ – see front matter © 2012 Published by Elsevier Ltd.
http://dx.doi.org/10.1016/j.parkreldis.2012.06.019

a major cause of both frontotemporal lobar degeneration (FTLD) and amyotrophic lateral sclerosis (ALS) [4,5].

Each of these genes can be associated with multiple clinical entities. Patients with *MAPT* mutations may receive diagnoses of frontotemporal dementia (FTD), primary progressive aphasia (PPA), or progressive supranuclear palsy (PSP). Rarely, corticobasal syndrome (CBS) or FTD with ALS (FTD-ALS) may be manifested in these patients [6]. The clinical diagnoses of patients with *PGRN* mutations include FTD, PPA, and CBS [6]. *C9orf72* repeat expansion causes FTD, ALS, FTD-ALS [4,5], PPA [5,7], and CBS [8] phenotypes. Thus, due to the complicated and often overlapping genetic and phenotypic variability in these patients, an accurate diagnosis of these clinical entities before autopsy is often difficult for clinicians.

To date, few comprehensive screening studies of these three genes have been performed in Asian populations. The aims of this study are to characterize the roles of known and, more importantly, novel disease-causing genes and to investigate the genetic and clinical features of FTLD, PSP, and CBS patients with *MAPT*, *PGRN*, and *C9orf72* mutations. In this study, we also describe the abnormal eye movements that are generally not observed in sporadic PSP but occur in early-onset PSP patients bearing *MAPT* mutations.

2. Methods

2.1. Subjects

We studied 75 Japanese patients who were diagnosed with FTLD, PSP, and CBS with or without a family history of disease. FTLD was divided into three subclasses: behavioral variant FTD (bvFTD), FTD-ALS, and PPA. The clinical diagnoses were established according to the consensus criteria for FTD [9], PPA [10], PSP [11], and CBS [12]. The characteristics of the 75 analyzed patients (69 index patients) are shown in Table 1. This study was approved by the ethics committee of the Juntendo University School of Medicine. Each subject provided written informed consent. All of the subjects in the control cohort were Japanese individuals and were evaluated by neurologists to ensure that no subjects exhibited any clinical manifestations of neurodegenerative diseases.

2.2. Genetic analyses

For direct sequence analysis, each exon was amplified by polymerase chain reaction (PCR) using published primers for *MAPT* [13] and *PGRN* [2] in a standard protocol. Dideoxy cycle sequencing was performed using Big Dye Terminator chemistry (Applied Biosystems, Foster City, CA). These products were loaded into ABI310 and 3130 automated DNA sequence analyzers and analyzed with DNA Sequence Analysis software (Applied Biosystems). To provide a qualitative assessment of the presence of an expanded $(GGGGCC)_n$ hexanucleotide repeat in the *C9orf72* gene, we performed repeat-primed PCR as previously described [4]. The normal repeat number of the GGGGCC hexanucleotide was determined in all of the patients using genotyping primers, as previously described [4]. The PCR products were analyzed on an ABI3130 DNA Analyzer and visualized using Gene Mapper software (Applied Biosystems).

Table 1
The clinical diagnoses and characteristics of 75 patients (69 index patients).

Clinical phenotype	No.	% of total	% of Male	Mean (SD) AAO (range, years)	Familial	Sporadic
FTLD	38	50.7	39.5	57.1 (±12.4), 36–78	21	17
bvFTD	29	38.7	34.5	54.5 (±12.6), 36–78	18	11
FTD-ALS	2	2.7	100	67.5 (±1.5), 66–69	1	1
PPA	7	9.3	42.9	65.0 (±7.4), 58–77	2	5
PSP	25	33.3	68.0	59.8 (±13.0), 40–76	18	7
CBS	12	16.0	33.3	58.4 (±9.52), 40–71	9	3
Total	75	100	48.0	58.2 (±12.3), 36–78	48	27
Index patients	69	92.0	46.4	58.9 (±12.4), 36–78	42	27
Relatives	6	8	66.7	50.3 (±6.6), 44–61	6	0

FTLD = frontotemporal lobar degeneration.
bvFTD = behavioral variant frontotemporal dementia.
FTD-ALS = frontotemporal dementia with amyotrophic lateral sclerosis.
PPA = primary progressive aphasia; PSP = progressive supranuclear palsy.
CBS = corticobasal syndrome; SD = standard deviation; AAO = age at onset.

2.3. Multiplex ligation-dependent probe amplification (MLPA)

To confirm the gene dosages of *MAPT* and *PGRN*, we performed MLPA using the SALSA MLPA P275-B1 MAPT-PGRN kit (MRC-Holland, Amsterdam, The Netherlands). The DNA detection/quantification protocol was provided by the manufacturer. The products were quantified using the ABI3130 Genetic Analyzer and Gene Mapper v3.7 (Applied Biosystems). The kit contains 32 probes, including 13 *MAPT* probes (located in exons 1–13) and 5 *PGRN* probes (located in exons 1, 3, 6, 10, and 12) located within other genes on chromosome 17q21. The MLPA data were analyzed as described previously [14].

2.4. Exon-trapping analysis

To determine whether a novel *MAPT* mutation was pathogenic, we performed an exon-trapping analysis. We used a wild-type construct and constructs containing the novel *MAPT* p.S285R or the IVS10+3 intronic mutation [15]. The *MAPT* sequences included exon 10, 34 nucleotides of the upstream intronic sequence and 85 nucleotides of the downstream intronic sequence. The PCR products were subcloned into the splicing vector pSPL3 (Invitrogen, Carlsbad, CA), and exon trapping was performed as described previously [15].

2.5. Paternity testing

Microsatellite analysis with 10 markers (D2S293, D3S3521, D4S2971, D5S495, D6S16171, D7S2459, D8S1705, D16S430, D18S450, and D20S842) was performed in Patient 1 and his parents to confirm paternity.

2.6. TA cloning

The novel *PGRN* heterozygous deletion/insertion found in this study, *PGRN* p.G338RfsX23 (c.1012_1013delGGinsC), was confirmed by cloning the PCR products into the pCR4-TOPO Vector using the TOPO TA Cloning kit (Invitrogen) and sequencing the two haplotypes of the heterozygote.

3. Results

3.1. Results of MAPT analysis

3.1.1. Genetic and molecular analyses of MAPT

In this study, we identified nine patients with *MAPT* mutations from six families. Four heterozygous missense mutations in *MAPT*, p.L266V, p.N279K, p.N296N, and the novel p.S285R (Supplementary Fig. 1), were identified by direct sequencing. None of the 182 normal Japanese controls included in this study had the *MAPT* p.S285R. In addition, we examined the amino acid sequences of the MAPT protein in other species and found that the site of the p.S285R mutation was highly conserved (see Supplementary Fig. 2). The novel p.S285R mutation in *MAPT* was detected in Patient 1 but not in his parents (Fig. 1A and Supplementary Fig. 1). The parentage of this patient and the DNA authenticity were confirmed using a microsatellite panel (see Supplementary Table 1). These results suggest that p.S285R is a *de novo* mutation. To investigate whether the p.S285R mutation is pathogenic, we performed an exon-trapping analysis. The p.S285R mutation produced a marked increase in the splicing of exon 10 (Fig. 1B) and resulted in the overproduction of tau isoforms that contain 4-repeat tau, such as IVS10+3 [15]. These results indicate that the p.S285R mutation is a novel, *de novo* pathogenic mutation. Previously, p.L266V, p.N279K, and p.N296N had been reported as pathogenic mutations [16–18].

Table 2 lists the clinical features of all of the *MAPT*- and *PGRN*-positive patients in this study, and Supplementary Fig. 3 shows Pedigrees C, D, E, F, and G. The average age at disease onset of patients with a single heterozygous *MAPT* mutation was 42.3 ± 2.9 (range: 37–46) years. MLPA analysis showed no gene dosage abnormalities (multiplications or deletions) in *MAPT* in this cohort.

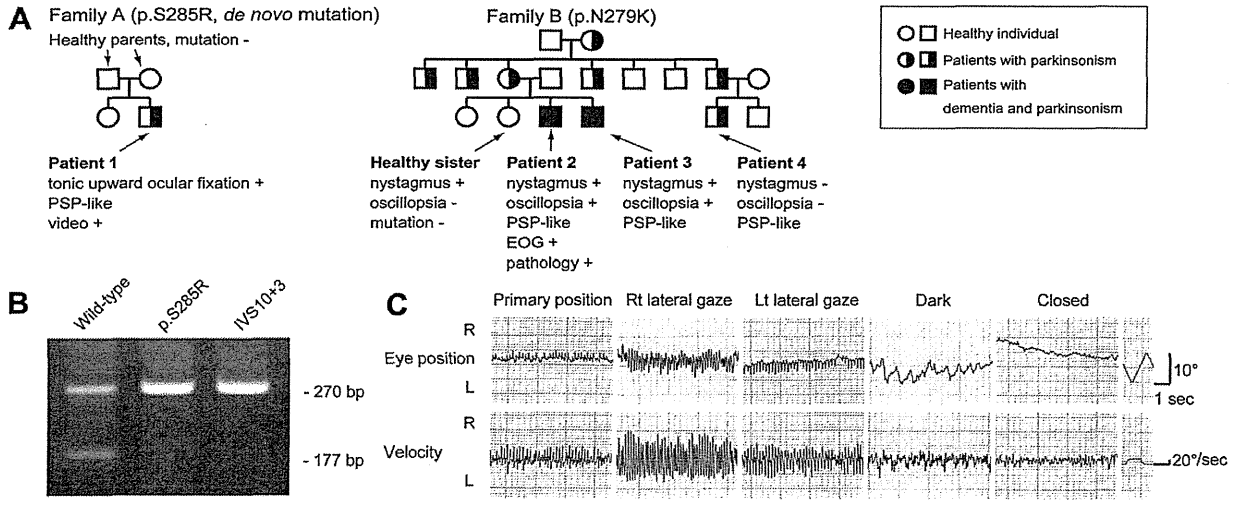

Fig. 1. (A) The pedigrees of families A and B. (B) Exon-trapping analysis for the effects of the *MAPT* p.S285R mutation on exon 10 splicing. (C) Horizontal electro-oculogram recordings in Patient 2.

3.1.2. Clinical presentations of MAPT-positive patients with the abnormal eye movements that are generally not observed in patients with sporadic PSP

3.1.2.1. Patient 1 (MAPT p.S285R). This patient was a 46-year-old man who presented with difficulty speaking and breathing. The patient had no family history of dementia or movement disorders (Fig. 1A). A physical examination revealed gait disturbance, limb bradykinesia, and frequent falling. At age 47, the patient exhibited palilalia and a mild obsession with eating. The patient's Mini-Mental State Examination (MMSE) score was 28/30, but his Frontal Assessment Battery score was 12/18. The patient exhibited a slowing of saccadic eye movements with a relative preservation of smooth pursuit, vertical supranuclear gaze palsy, and tonic upward ocular fixation (see Video Supplement); when the patient's eyes opened after closing, they remained fixated upward and could not be moved voluntarily to the primary position (i.e., Bell's phenomenon remained). To overcome this disability, the patient extended his neck, which resulted in a reflex downward movement of the eyes (the vestibulo-ocular reflex), and next he slightly flexed his neck to a neutral position with his eyes in the primary position. Later, the patient developed bradykinesia and postural instability with frequent falling. L-dopa/benserazide (up to 900 mg/day) was ineffective. The patient's condition gradually deteriorated, and he developed dementia, retrocollis, vertical and horizontal supranuclear palsy, and bradykinesia. At age 49, the patient died of suffocation from the aspiration of food material. No autopsy was performed. The clinical diagnosis was probable PSP.

3.1.2.2. Patient 2 (MAPT p.N279K). This patient was the older brother of Patient 3 (Fig. 1A). Patient 2 was a 42-year-old man who exhibited oscillopsia, micrographia, and a shuffling gait. This patient reported having had nystagmus without oscillopsia since childhood. A neurological examination revealed marked horizontal nystagmus. The patient's pupils were isocoric, and his visual acuity was normal. The patient presented with rigidity, bradykinesia, and postural tremor in the upper limbs. Electro-oculography revealed horizontal pendular nystagmus in the primary position and in all gaze directions (Fig. 1C). L-dopa/benserazide at 200 mg/day mildly alleviated his parkinsonism. Two years later, the patient developed prominent postural instability and became prone to falling. Upward and downward gaze palsy and apraxia of eyelid opening were also noted. At that time, the clinical diagnosis was possible PSP with a family history of dementia and parkinsonism. The patient's cognitive function deteriorated gradually. At age 52, he was bedridden and required a gastrostomy. The patient died of pneumonia at age 54. A postmortem pathological examination of the brain revealed mild atrophy of the frontal lobe and the tegmentum of the midbrain and pons. Microscopic analysis showed severe degenerative changes in the substantia nigra and the subcortical nuclei. Immunohistochemistry using anti-phosphorylated tau (p-tau) antibodies revealed numerous tau-positive neuronal and glial inclusions in the frontotemporal cortex, white matter, and the subcortical nuclei (see Supplementary Fig. 4). These p-tau deposits reacted with anti-4-repeat tau antibodies but not with anti-3-repeat tau antibodies.

3.1.2.3. Patient 3 (MAPT p.N279K). This patient was the younger brother of Patient 2 (Fig. 1A). At age 44, Patient 3 noticed clumsiness in his right hand and oscillopsia. The patient reported having nystagmus since childhood. A neurological examination revealed large, horizontal pendular nystagmus in the primary position and in all gaze directions. The patient's visual acuity, pupils, and light reflexes were all normal. Mild bradykinesia and rigidity in the neck and the right upper limb were noted. Postural tremor in both hands and the tongue and postural instability were observed. Treatment with 600 mg/day of L-dopa/carbidopa was not effective. The patient's oscillopsia gradually worsened, and eventually he was unable to read printed materials. At age 47, the patient developed upward and downward gaze palsy, slowing of saccades, and apraxia of eyelid opening. The patient had prominent postural instability and was prone to falling. The patient's first clinical diagnosis was possible PSP with a family history of dementia and parkinsonism. The patient died at age 56. An autopsy was not performed.

3.1.2.4. Patients 5, 6, and 7 (MAPT p.N279K). The clinical presentations of these three patients have been described previously [19]. All three patients had clinical diagnoses of possible PSP (Table 2) and visual grasping [19,20].

3.2. Results of PGRN analysis

3.2.1. Genetic Analyses of PGRN

We identified one patient with a *PGRN* mutation (Table 2, Supplementary Fig. 3). One novel heterozygous deletion/insertion

Table 2
Clinical features of patients with *MAPT* and *PGRN* mutations.

Family	A	B			C	D		E	F	G
Patient	1	2	3	4	5	6	7	8	9	10
Gene					*MAPT*					*PGRN*
Genotyping					Heterozygous					
Nucleotide change	c.853A > C	c.837T > G	c.837T > G	c.837T > G	c.837T > G	c.837T > G	c.837T > G	c.796C > G	c.888T > C	c.1012_1013delGGinsC
Amino acid change	p.S285R	p.N279K	p.N279K	p.N279K	p.N279K	p.N279K	p.N279K	p.L266V	p.N296N	p.G338RfsX23
Exon	10	10	10	10	10	10	10	9	10	9
Mode of inheritance	*de novo*	AD	AD	AD	NA	AD	AD	AD	AD	AD
Age at onset, years	46	42	44	46	41	42	43	37	44	59
Age at evaluation, years	47	47	45	50	44	44	45	38	49	61
Age at death, years	49	54	56	alive	51	54	51	alive	alive	alive
Sex	M	M	M	M	F	F	F	F	M	F
Clinical syndromes	PSP	PSP	PSP	PSP	PSP	PSP	PSP	bvFTD	PSP	PPA
Clinical features										
Initial symptoms	P	P	P	P	P	P	P	dementia	P	aphasia
Personality/behavior changes	−	+	−	−	−	−	−	+	+	−
Mini mental state examination score	28/30	NA	NA	28/30	NA	NA	NA	0	24/30	29/30
Hasegawa dementia scale-revised[a]	NA	18/30	NA	NA	21/30	28/30	30/30	0	21/30	29/30
Nonfluent spontaneous speech	−	−	−	−	−	−	−	−	−	+
Apraxia of eyelid opening	−	+	+	+	+	+	+	−	−	−
Abnormal eye movements										
Supranuclear gaze palsy	+	+	+	+	+	+	+	−	+	−
Tonic upward ocular fixation	+	−	−	−	−	−	−	−	−	−
Oscillopsia with CN	−	+	+	−	−	−	−	−	−	−
Visual grasping	−	−	−	−	+	+	+	−	−	−
Parkinsonism										
Bradykinesia	+	+	+	+	+	+	+	−	+	−
Rigidity	−	+	+	+	+	+	+	−	+	−
Tremor	−	+	+	−	−	−	−	−	−	−
Postural instability	+	+	+	+	+	+	+	−	+	−
Response to L-dopa	−	partial[b]	−	partial[b]	partial[b]	partial[b]	partial[b]	NA	+	NA
Pyramidal sign	+	−	NA	−	+	−	+	+	+	−
Features of motor neuron disease	−	−	−	−	−	−	−	−	−	−
Reference					[19]	[19]	[19]			

AD = autosomal dominant.
P = parkinsonism; NA = not available.
CN = congenital nystagmus; PSP = progressive supranuclear palsy.
bvFTD = behavioral variant frontotemporal dementia; PPA = primary progressive aphasia.
[a] The Hasegawa dementia scale-revised is a brief dementia screening scale. The maximum score of the Hasegawa dementia scale-revised is 30 points. There was a significant difference in the mean score between the demented and non-demented subjects when the cut-off point was set at 20/21 [31].
[b] A partial response to L-dopa indicates that L-dopa was effective only in the early stages.

mutation in *PGRN*, p.G338RfsX23 (c.1012_1013delGGinsC), was detected by direct sequencing and TOPO TA cloning sequencing (Supplementary Fig. 1). None of the 182 normal Japanese controls included in this study had the *PGRN* p.G338RfsX23 (c.1012_1013delGGinsC) mutations. The age at disease onset of the patient with the heterozygous *PGRN* deletion/insertion was 59 years. Novel *PGRN* variants with unknown significance, p.R18Q and p.N118del, are listed in Table 3. MLPA analysis showed no gene dosage abnormalities in *PGRN*.

3.2.2. A clinical presentation of a novel PGRN mutation

3.2.2.1. Patient 10 (PGRN p.G338RfsX23, c.1012_1013delGGinsC). This patient, a 59-year-old woman, developed word-finding difficulties and underwent surgical clipping at age 54 for an unruptured

Table 3
Novel variants with unknown significance.

Gene	Nucleotidechange	Amino acid change	Exon	Amino acid conservation	Mean AAO (years)	Frequency		*P* value	Clinical diagnosis
						Patients *N* (%)	Controls *N* (%)		
PGRN	c.56G > A	p.R19Q	1	not conserved	66	1/69 (1.4)	0/186 (0)	0.605	PSP ($n = 1$)
PGRN	c.352_354delAAC	p.N118del	4	not conserved	53	3/69 (4.3)	3/272 (1.1)	0.187	bvFTD ($n = 3$)

AAO = age at onset.
PSP = progressive supranuclear palsy.
bvFTD = behavioral variant frontotemporal dementia.

aneurysm of the left middle cerebral artery. The patient's mother suffered from dementia, but the details of her disease were unknown. The patient substituted words for names of people and objects. Two years after the onset of symptoms, the patient became severely disfluent. However, she did not show any violent behavior, personality changes, or other behavioral abnormalities. The patient scored 29/30 on the MMSE. On the frontal assessment battery, she scored 13/18. The patient's time to complete the Trail Making Test (TMT) A was 70 s, and she could not finish the TMT B within five minutes. Her spontaneous speech production was characterized by slow and hesitant speech, frequently interrupted by long word-finding pauses. Her motor speech abilities were within the normal limits, and no apraxia of speech was noted. No parkinsonism was observed. The patient's clinical diagnosis was PPA with a family history of dementia.

3.3. Results of C9orf72 analysis

We identified no patients with expanded hexanucleotide repeats in *C9orf72* in this study. In 75 patients, the average repeat number based on fluorescent fragment-length analysis was 3.77 ± 2.56 (range 2–11 repeats). We have previously reported that an analysis of 197 Japanese healthy controls did not find any *C9orf72* mutation. The average repeat number was 3.69 ± 2.46 (range 2–14 repeats) in the 197 controls [21].

4. Discussion

We identified five *MAPT* mutations, including a novel *de novo* mutation and a novel *PGRN* mutation, and we found no *C9orf72* mutations in our 75 patients. More mutations were found in *MAPT* than in the other two genes evaluated in this study. The infrequent observation of *PGRN* and *C9orf72* mutations might be partly due to the small number of FTLD patients included ($n = 38$) because the majority of *PGRN* and *C9orf72* mutations have been described in patients with FTLD. In contrast to most other mutation screening studies, we performed MLPA analysis to ensure that exonic or larger deletions or multiplications of *MAPT* and *PGRN* would be identified. Therefore, our data also show that multiplications of *MAPT* and exonic or genomic deletions in *PGRN* are rare in Asian populations. Although mutations were detected in FTLD and PSP patients, we did not find any mutations in our CBS patients. A further larger study and investigation of the other genes are needed to clarify the genetic background of Japanese patients with CBS.

The *MAPT* p.S285R mutation, which we found in this study, is a novel *de novo* mutation. To the best of our knowledge, this report is the first description of an adult sporadic case of a *de novo MAPT* mutation associated with dementia and parkinsonism. All six patients (Patients 1, 2, 3, 5, 6, and 7) with PSP and the distinct eye movements described in the present study (such as tonic upward ocular fixation, oscillopsia with congenital nystagmus, and visual grasping) harbored *MAPT* mutations. Below, we discuss these abnormal eye movements, which are generally not observed in patients with sporadic PSP.

In Patient 1 (*MAPT* p.S285R), we observed tonic upward ocular fixation, which is a loss of downward saccades resembling an acquired ocular motor apraxia [22]. This condition is characterized by a loss of voluntary control of saccades and pursuit, whereas reflex movements—in particular, the vestibulo-ocular reflex—were preserved. Acquired ocular motor apraxia is usually the result of bilateral frontal or frontoparietal infarcts. Therefore, tonic upward ocular fixation due to a *MAPT* mutation might share "supranuclear" cerebral lesions in common with ocular motor apraxia. Brainstem functions, including the vestibulo-ocular reflex and Bell's phenomenon, were preserved in Patient 1.

In Patients 2 and 3 (*MAPT* p.N279K), pendular nystagmus was present since childhood and was suppressed with eyelid closure. These features are consistent with congenital nystagmus [23]. Most patients with congenital nystagmus do not complain of oscillopsia, despite having nearly continuous eye movement [23]. Notably, Patients 2 and 3 noticed oscillopsia when they developed parkinsonism. In these siblings, cerebral lesions caused solely by a *MAPT* mutation were unlikely to be the cause of their nystagmus; however, the co-existence of congenital nystagmus and the *MAPT* mutation might have caused the oscillopsia. This notion is supported in part because the patients had a sister who remained healthy — even in her late 60s — and did not complain of oscillopsia, despite having obvious pendular nystagmus (Fig. 1A). Thus, *MAPT* mutations might impair the visual-motion processing pathways that would normally suppress oscillopsia in patients with common congenital nystagmus. Visual grasping, which was first described by Ghika et al. [20], was observed in Patients 5, 6, and 7 (*MAPT* p.N279K) [19].

Although PSP is a rare manifestation of *MAPT* mutation [24], and the routine screening of sporadic PSP for mutations in *MAPT* is not recommended because of low yield [25], it is recommended that screening be considered for families in which there is an autosomal dominant history of a PSP syndrome, particularly when there are accompanying features suggestive of bvFTD [24]. The clinical difference from sporadic PSP might sometimes be difficult to detect, especially in patients without a family history [26–28]; however, an important case report indicated that an age at disease onset under 50 years combined with the absence of early falling may indicate a possible *MAPT* mutation in clinically diagnosed PSP, even in the absence of a positive family history [26]. Consistent with this observation, our eight *MAPT*-positive patients with PSP phenotype were younger than 50 years at disease onset (Table 2). We further suggest that it may be useful to test for *MAPT* mutations in early-onset PSP patients with the abnormal eye movements that are not typical of sporadic PSP. In fact, we identified the novel *de novo* mutation p.S285R in Patient 1 and p.N279K in Patient 5, who had no family history, after focusing on these clinical phenotypes.

To the best of our knowledge, the *PGRN* mutation has not been previously described in Asian populations [29]. We detected a novel *PGRN* mutation, p.G338RfsX23 (c.1012_1013delGGinsC), and thus showed that *PGRN* mutations may exist in Asian populations. This mutation introduces a premature termination codon at the same site as the p.G333VfsX28 (c.998delG) mutation, which was reported previously, and produced a PPA phenotype in all of the affected individuals [30]. The PPA phenotype of p.G338RfsX23 (c.1012_1013delGGinsC) in our study is remarkably similar to that of p.G333VfsX28 (c.998delG), especially in the manifestation of word-finding and object-naming difficulties and the lack of memory or personality changes during the first few years after symptom onset. We believe that the mutant RNA in both cases is most likely subjected to nonsense-mediated decay, similar to other *PGRN* mutations [2].

In summary, based on these findings, we recommend genetic testing for *MAPT* mutations not only in familial patients but also in sporadic patients, especially early-onset PSP patients with the abnormal eye movements that are generally not observed in sporadic PSP. Although *PGRN* and *C9orf72* mutations were rare in this study, we determined that the *PGRN* mutation does exist in Asian patients with FTLD (PPA). Based on the clinical information, screening for *MAPT*, *PGRN*, and *C9orf72* mutations should be further undertaken to improve the diagnosis of specific clinical entities of neurodegenerative disorders.

Conflicts of interest

None.

Acknowledgments

The authors thank all of the participants in this study. The authors also thank Dr. Mariely DeJesus-Hernandez for technical advice on the analysis of *C9orf72* repeat expansion. This work was supported by the Strategic Research Foundation Grant-in-Aid Project for Private Universities, Grants-in-Aid for Scientific Research, Grant-in-Aid for Young Scientists, and Grant-in-Aid for Scientific Research on Innovative Areas from the Japanese Ministry of Education, Culture, Sports, Science and Technology, Grants-in-Aid from the Research Committee of CNS Degenerative Diseases and Muro Disease (Kii ALS/PDC), Grants-in-Aid from the Research Committee on CNS Degenerative Diseases and Perry Syndrome from the Ministry of Health, Labor and Welfare of Japan, Project Research Grants-in-Aid from Juntendo University School of Medicine, and CREST from the Japan Science and Technology Agency (JST).

Appendix A. Supplementary data

Supplementary data related to this article can be found online at http://dx.doi.org/10.1016/j.parkreldis.2012.06.019.

References

[1] Hutton M, Lendon CL, Rizzu P, Baker M, Froelich S, Houlden H, et al. Association of missense and 5'-splice-site mutations in tau with the inherited dementia FTDP-17. Nature 1998;393:702–5.
[2] Baker M, Mackenzie IR, Pickering-Brown SM, Gass J, Rademakers R, Lindholm C, et al. Mutations in progranulin cause tau-negative frontotemporal dementia linked to chromosome 17. Nature 2006;442:916–9.
[3] Cruts M, Gijselinck I, van der Zee J, Engelborghs S, Wils H, Pirici D, et al. Null mutations in progranulin cause ubiquitin-positive frontotemporal dementia linked to chromosome 17q21. Nature 2006;442:920–4.
[4] Dejesus-Hernandez M, Mackenzie IR, Boeve BF, Boxer AL, Baker M, Rutherford NJ, et al. Expanded GGGGCC hexanucleotide repeat in noncoding region of C9ORF72 causes chromosome 9p-linked FTD and ALS. Neuron 2011; 72:245–56.
[5] Renton AE, Majounie E, Waite A, Simon-Sanchez J, Rollinson S, Gibbs JR, et al. A hexanucleotide repeat expansion in C9ORF72 is the cause of chromosome 9p21-Linked ALS-FTD. Neuron 2011;72:257–68.
[6] Boeve BF, Hutton M. Refining frontotemporal dementia with parkinsonism linked to chromosome 17: introducing FTDP-17 (MAPT) and FTDP-17 (PGRN). Arch Neurol 2008;65:460–4.
[7] Murray ME, Dejesus-Hernandez M, Rutherford NJ, Baker M, Duara R, Graff-Radford NR, et al. Clinical and neuropathologic heterogeneity of c9FTD/ALS associated with hexanucleotide repeat expansion in C9ORF72. Acta Neuropathol 2011;122:673–90.
[8] Lindquist S, Duno M, Batbayli M, Puschmann A, Braendgaard H, Mardosiene S, et al. Corticobasal and ataxia syndromes widen the spectrumof C9ORF72 hexanucleotide expansion disease. Clin Genetics 2012 May 31 [Epub ahead of print].
[9] Neary D, Snowden JS, Gustafson L, Passant U, Stuss D, Black S, et al. Frontotemporal lobar degeneration: a consensus on clinical diagnostic criteria. Neurology 1998;51:1546–54.
[10] Mesulam MM. Slowly progressive aphasia without generalized dementia. Ann Neurol 1982;11:592–8.
[11] Litvan I, Agid Y, Calne D, Campbell G, Dubois B, Duvoisin RC, et al. Clinical research criteria for the diagnosis of progressive supranuclear palsy (Steele-Richardson-Olszewski syndrome): report of the NINDS-SPSP international workshop. Neurology 1996;47:1–9.
[12] Boeve BF, Lang AE, Litvan I. Corticobasal degeneration and its relationship to progressive supranuclear palsy and frontotemporal dementia. Ann Neurol 2003;54(Suppl. 5):S15–9.
[13] Baker M, Kwok JB, Kucera S, Crook R, Farrer M, Houlden H, et al. Localization of frontotemporal dementia with parkinsonism in an Australian kindred to chromosome 17q21-22. Ann Neurol 1997;42:794–8.
[14] Keyser RJ, Lombard D, Veikondis R, Carr J, Bardien S. Analysis of exon dosage using MLPA in South African Parkinson's disease patients. Neurogenetics 2010;11:305–12.
[15] Varani L, Hasegawa M, Spillantini MG, Smith MJ, Murrell JR, Ghetti B, et al. Structure of tau exon 10 splicing regulatory element RNA and destabilization by mutations of frontotemporal dementia and parkinsonism linked to chromosome 17. Proc Natl Acad Sci U S A 1999;96:8229–34.
[16] Kobayashi T, Ota S, Tanaka K, Ito Y, Hasegawa M, Umeda Y, et al. A novel L266V mutation of the tau gene causes frontotemporal dementia with a unique tau pathology. Ann Neurol 2003;53:133–7.
[17] Clark LN, Poorkaj P, Wszolek Z, Geschwind DH, Nasreddine ZS, Miller B, et al. Pathogenic implications of mutations in the tau gene in pallido-ponto-nigral degeneration and related neurodegenerative disorders linked to chromosome 17. Proc Natl Acad Sci U S A 1998;95:13103–7.
[18] Spillantini MG, Yoshida H, Rizzini C, Lantos PL, Khan N, Rossor MN, et al. A novel tau mutation (N296N) in familial dementia with swollen achromatic neurons and corticobasal inclusion bodies. Ann Neurol 2000;48:939–43.
[19] Ogaki K, Motoi Y, Li Y, Tomiyama H, Shimizu N, Takanashi M, et al. Visual grasping in frontotemporal dementia and parkinsonism linked to chromosome 17 (microtubule-associated with protein tau): a comparison of N-Isopropyl-p-[(123)I]-iodoamphetamine brain perfusion single photon emission computed tomography analysis with progressive supranuclear palsy. Mov Disord 2011;26:561–3.
[20] Ghika J, Tennis M, Growdon J, Hoffman E, Johnson K. Environment-driven responses in progressive supranuclear palsy. J Neurol Sci 1995;130:104–11.
[21] Ogaki K, Li Y, Atsuta N, Tomiyama H, Funayama M, Watanabe H, et al. Analysis of C9orf72 repeat expansion in 563 Japanese patients with ALS. Neurobiol Aging 2012 June 21 [Epub ahead of print].
[22] Pierrot-Deseilligny C, Gautier JC, Loron P. Acquired ocular motor apraxia due to bilateral frontoparietal infarcts. Ann Neurol 1988;23:199–202.
[23] Leigh RJZD. In: The neurology of eye movements. 4 ed. New York: Oxford University Press; 2006. p. 512–21, 638–45.
[24] Rohrer JD, Paviour D, Vandrovcova J, Hodges J, de Silva R, Rossor MN. Novel L284R MAPT mutation in a family with an autosomal dominant progressive supranuclear palsy syndrome. Neurodegener Dis 2011;8:149–52.
[25] Williams DR, Pittman AM, Revesz T, Lees AJ, de Silva R. Genetic variation at the tau locus and clinical syndromes associated with progressive supranuclear palsy. Mov Disord 2007;22:895–7.
[26] Morris HR, Osaki Y, Holton J, Lees AJ, Wood NW, Revesz T, et al. Tau exon 10 + 16 mutation FTDP-17 presenting clinically as sporadic young onset PSP. Neurology 2003;61:102–4.
[27] Rossi G, Gasparoli E, Pasquali C, Di Fede G, Testa D, Albanese A, et al. Progressive supranuclear palsy and Parkinson's disease in a family with a new mutation in the tau gene. Ann Neurol 2004;55:448.
[28] Ros R, Thobois S, Streichenberger N, Kopp N, Sanchez MP, Perez M, et al. A new mutation of the tau gene, G303V, in early-onset familial progressive supranuclear palsy. Arch Neurol 2005;62:1444–50.
[29] Kim HJ, Jeon BS, Yun JY, Seong MW, Park SS, Lee JY. Screening for MAPT and PGRN mutations in Korean patients with PSP/CBS/FTD. Parkinsonism Relat Disord 2010;16:305–6.
[30] Mesulam MM. Primary progressive aphasia—a language-based dementia. N Engl J Med 2003;349:1535–42.
[31] Imai Y, Hasegawa K. The revised hasegawa's dementia scale (HDS-R) – evaluation of its usefulness as a screening test for dementia. J Hong Kong Coll Psychiatr 1994;4:20–4.

SCIENTIFIC REPORTS

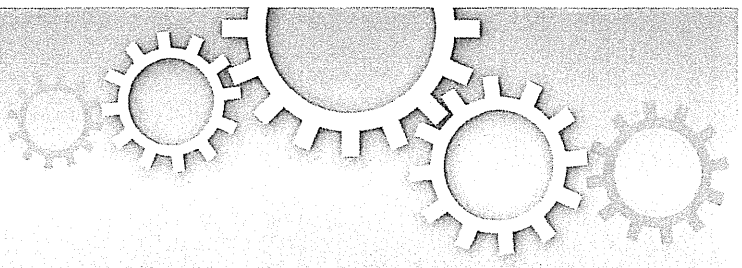

OPEN

SUBJECT AREAS:
MITOPHAGY
PHOSPHORYLATION
CELL DEATH IN THE NERVOUS SYSTEM
UBIQUITIN LIGASES

Received
3 August 2012

Accepted
5 December 2012

Published
19 December 2012

Correspondence and requests for materials should be addressed to Y.I. (yzimai@juntendo.ac.jp) or N.H. (nhattori@juntendo.ac.jp)

PINK1-mediated phosphorylation of the Parkin ubiquitin-like domain primes mitochondrial translocation of Parkin and regulates mitophagy

Kahori Shiba-Fukushima[1], Yuzuru Imai[2], Shigeharu Yoshida[3], Yasushi Ishihama[3], Tomoko Kanao[4], Shigeto Sato[1] & Nobutaka Hattori[1,2,4,5]

[1]Department of Neurology, Juntendo University Graduate School of Medicine, Tokyo 113-8421, Japan, [2]Department of Neuroscience for Neurodegenerative Disorders, Juntendo University Graduate School of Medicine, Tokyo 113-8421, Japan, [3]Department of Molecular and Cellular BioAnalysis, Graduate School of Pharmaceutical Sciences, Kyoto University, Kyoto 606-8501, Japan, [4]Research Institute for Diseases of Old Age, Juntendo University Graduate School of Medicine, Tokyo 113-8421, Japan, [5]CREST (Core Research for Evolutionary Science and Technology), JST, Saitama 332-0012, Japan.

Parkinson's disease genes *PINK1* and *parkin* encode kinase and ubiquitin ligase, respectively. The gene products PINK1 and Parkin are implicated in mitochondrial autophagy, or mitophagy. Upon the loss of mitochondrial membrane potential ($\Delta\Psi$m), cytosolic Parkin is recruited to the mitochondria by PINK1 through an uncharacterised mechanism – an initial step triggering sequential events in mitophagy. This study reports that Ser65 in the ubiquitin-like domain (Ubl) of Parkin is phosphorylated in a PINK1-dependent manner upon depolarisation of $\Delta\Psi$m. The introduction of mutations at Ser65 suggests that phosphorylation of Ser65 is required not only for the efficient translocation of Parkin, but also for the degradation of mitochondrial proteins in mitophagy. Phosphorylation analysis of Parkin pathogenic mutants also suggests Ser65 phosphorylation is not sufficient for Parkin translocation. Our study partly uncovers the molecular mechanism underlying the PINK1-dependent mitochondrial translocation and activation of Parkin as an initial step of mitophagy.

Mutations of the *PINK1* gene cause selective degeneration of the midbrain dopaminergic neurons in autosomal recessive juvenile Parkinson's disease (PD)[1]. The *PINK1* gene encodes a serine/threonine kinase with a predicted mitochondrial target sequence and a putative transmembrane domain at the N-terminus[2–5]. Loss of the *PINK1* gene in *Drosophila* results in the degeneration of mitochondria in cells with high energy demands, such as muscle and sperm cells, which is suppressed by the introduction of the *parkin* gene, another gene responsible for autosomal recessive juvenile PD[6–8]. The gene product Parkin encodes a RING-finger type ubiquitin ligase (E3) with a Ubl domain at the N-terminus[9–12].

A series of cell biological studies have provided strong evidence that there are important roles for PINK1 and Parkin in regulating mitochondrial homeostasis. PINK1 is constitutively proteolysed by the mitochondrial rhomboid protease, PARL, at the mitochondrial membrane of healthy mitochondria, resulting in processed forms of PINK1[13–16]. The processed PINK1 is rapidly degraded by the proteasome[2,17]. The reduction of $\Delta\Psi$m leads to the accumulation and activation of PINK1 in the mitochondria[17–19] through a currently unresolved mechanism[20]. The accumulation of PINK1 recruits Parkin from the cytosol to the mitochondria with decreased membrane potential, which stimulates Parkin E3 activity, promoting mitochondrial degradation via an autophagic event known as mitophagy[17,21–24]. The recruitment of cytosolic Parkin to the mitochondria upon disruption of $\Delta\Psi$m is believed to be the first step of mitophagy for the removal of damaged mitochondria. This recruitment is required for the kinase activity of PINK1[17,21–25]. Although two separate studies have proposed that Parkin is directly phosphorylated by PINK1[26,27], others have failed to detect Parkin phosphorylation by PINK1[21], suggesting that the kinase activity of PINK1 itself is relatively low. One reason biochemical analysis has been unable to obtain direct evidence is that recombinant human PINK1 purified from mammalian cultured cells or bacteria easily loses kinase activity, while insect PINK1 has significant autophosphorylation activity[28,29].

Very recently, Kondapalli, C. *et al.* reported that PINK1 directly phosphorylates Parkin at Ser65 in the Ubl domain[18]. However, the extent and consequences of Parkin phosphorylation by PINK1 in mitochondrial regulation are still not fully understood.

To address this issue, we attempted to independently monitor and compare the phosphorylation status of Parkin in wild-type and *PINK1*-deficient cells, thereby excluding the possibility of phosphorylations by uncharacterised kinases other than PINK1[30]. Here, we also report that Parkin is demonstrably phosphorylated at Ser65 in a PINK1-dependent manner. Furthermore, we show that this phosphorylation event is implicated in the regulation of mitochondrial translocation of Parkin and the subsequent degradation of mitochondrial surface proteins during mitophagy.

Results

Parkin is phosphorylated upon depolarisation in ΔΨm. We used [^{32}P] orthophosphate to metabolically label mouse embryonic fibroblasts (MEFs) derived from *PINK1* deficient mice, in which HA-tagged Parkin together with FLAG-tagged wild-type or kinase-dead forms (triple mutant with K219A, D362A and D384A) of PINK1 were virally introduced (hereafter referred to as "PINK1-FLAG WT" or "KD/HA-Parkin/*PINK1*$^{-/-}$" MEFs) and then induced Parkin-mediated mitophagy via treatment with the protonophore carbonyl cyanide *m*-chlorophenyl hydrazone (CCCP). As shown in Figure 1a, Parkin was specifically phosphorylated in CCCP-treated PINK1-FLAG WT/HA-Parkin/*PINK1*$^{-/-}$ MEFs, but not in PINK1-FLAG KD/HA-Parkin/*PINK1*$^{-/-}$ MEFs. Phos-tag Western blotting, in which phosphorylated proteins appear as slower migrating bands[28], revealed that Parkin was phosphorylated within 10 min following CCCP treatment (Fig. 1b). Phosphorylation of Parkin reached its maximum level approximately 40 min after CCCP treatment and was sustained at least until 6 hr (Supplementary Fig. S1). Under these conditions, slower migrating bands of PINK1 also appeared, which very likely reflects the autophosphorylation of PINK1 when activated (Fig. 1b)[18]. The suppression of PINK1 accumulation by RNA interference suggested thatΔΨm depolarisation-dependent activation of PINK1 along with PINK1 accumulation is a key element for Parkin phosphorylation (Fig. 1c). Every PINK1 deletion and pathogenic mutant we tested failed to stimulate Parkin phosphorylation effectively, strongly suggesting that intact PINK1 is required for this action (Fig. 1d and e). Importantly, human fibroblasts from a patient with *PINK1*-linked parkinsonism also lacked the activity to phosphorylate Parkin (Fig. 1f). The phosphorylated Parkin disappeared within 30 min during the recovery of ΔΨm depolarisation by the removal of CCCP from the culture medium (Fig. 1g). Further analysis using phosphatase and proteasome inhibitors suggested that phosphorylated Parkin is at least partly degraded by proteasomal activity in the mitochondria (Supplementary Fig. S2).

Phosphorylation of Ser65 in the Parkin Ubl domain primes the mitochondrial translocation of Parkin. To determine which residue(s) of Parkin are phosphorylated, we immunopurified HA-tagged Parkin from PINK1-FLAG WT or KD/HA-Parkin/*PINK1*$^{-/-}$ MEFs treated with or without CCCP and performed mass spectrometric analysis for phospho-peptides (Supplementary Fig. S3). Although Phos-tag Western blotting of Parkin mainly detected a single band shift, which represents a single phospho-modification, the mass spectrometric analysis identified Ser9 or Ser10 and Ser65, Ser101 and Ser198 as phosphorylated residues of Parkin. Among these residues, only Ser65 phosphorylation increased (33-fold) in CCCP-treated PINK1-FLAG WT/HA-Parkin/*PINK1*$^{-/-}$ MEFs (Supplementary Fig. S3). Phos-tag Western blotting with mutant forms of Parkin, in which the identified phospho-serine residues are replaced with alanine, revealed that the band shift represents Ser65 phosphorylation (Fig. 2a). An *in vitro* kinase assay with recombinant insect PINK1, which has marked kinase activity[28], strongly suggested that PINK1 directly phosphorylates Parkin at Ser65 (Supplementary Fig. S4). The Ser65 residue lies in the Ubl domain and is highly conserved from human to *Drosophila* (Fig. 2b). We next examined whether phosphorylation of Ser65 is required for Parkin-mediated mitophagy. GFP-tagged Parkin WT, which was localised both in the cytoplasm and in the nuclei of mock (DMSO)-treated cells (0 hr, Fig. 2c and d), was translocated to the mitochondria and induced the perinuclear aggregation of mitochondria 2 hr after CCCP treatment, as previously reported (2 hr, Fig. 2c and d)[17,23]. Replacement of Ser65 with alanine (S65A) did not affect the subcellular localisation of Parkin in mock-treated cells when compared with that of GFP-Parkin WT (0 hr, Fig. 2c and d). However, GFP-Parkin S65A almost completely inhibited the mitochondrial translocation of Parkin and the perinuclear rearrangement of mitochondria 0.5 hr after CCCP treatment (0.5 hr, Fig. 2c and d) and showed delayed translocation in 2 hr (2 hr, Fig. 2c and d). The expression of a putative phosphomimetic Parkin S65E also showed a subcellular localisation similar to that of GFP-Parkin WT in both DMSO- and CCCP-treated cells (Fig. 2c). However, GFP-Parkin S65E exhibited a mild translocation defect, suggesting that S65E does not fully mimic the phosphorylated Ser65 (Fig. 2d).

Parkin Ser65 phosphorylation is not sufficient for mitochondrial translocation upon depolarisation of ΔΨm. As PINK1-mediated Ser65 phosphorylation appeared to be required for efficient translocation of Parkin, we next examined whether well-characterised pathogenic Parkin mutants were subjected to phosphorylation upon CCCP treatment. In this experiment, we used three kinds of Parkin mutants based on the previous and current studies (Supplementary Fig. S5)[17,22,23]. The first group, V15M, P37L, R42P and A46P, had intact or weakly impaired mitochondrial translocation activity. The second group, T415N and G430D, had mildly impaired translocation activity. The third group, K161N, K221N and T240R, almost completely lacked translocation activity (Fig. 3a). Surprisingly, all of the mutants possessed comparable phosphorylation efficiencies to those of WT (Fig. 3b). This result suggests that Ser65 phosphorylation is not sufficient for the mitochondrial translocation of Parkin.

Biochemical fractionation of endogenous Parkin from SH-SY5Y cells detected only the phosphorylated form of Parkin in the mitochondrial fraction upon CCCP treatment (Fig. 3c), which strongly suggests that phosphorylation of Parkin is required for mitochondrial translocation. There was a slight difference in the gel mobility of phosphorylated Parkin between the cytosolic and the mitochondrial fractions and between CCCP-treated periods of time. These differences very likely reflect differences in the complexity of the contents of each fraction rather than in the phosphorylation status of Parkin because a single shifted band appears in the mixed fractions (Mito + Cyto in Fig. 3c; CCCP 30 min + 60 min in Supplementary Fig. S6).

Effect of Parkin Ser65 phosphorylation on the autophagic reaction. We next examined whether Ser65 phosphorylation is required for the subsequent autophagic reaction, in which various ubiquitin-proteasome- and autophagy-related proteins are involved, including the 26S proteasome, p97/VCP, p62/SQSTM1, LC3, ATG5 and ATG7[22,23,31–35]. Parkin has been reported to be involved in the ubiquitin-proteasome-dependent degradation of a variety of mitochondrial outer membrane proteins, including Mitofusin1 (Mfn1)[32], Mfn2[32], Miro1[36,37], Miro2[37], VDAC1[22] and Tom20[31]. Degradation of Mfn1, VDAC1 and Tom20 at the mitochondrial outer membrane was observed in PINK1 WT/GFP-Parkin/*PINK1*$^{-/-}$ MEFs 1 to 4 hr after CCCP treatment (Fig. 4a). While GFP-Parkin harbouring S65A or S65E mutations was also capable of inducing Mfn1, VDAC1 and Tom20 degradation, the efficiency was impaired, especially in Mfn1 and VDAC1 (Fig. 4a). Long-term time course analysis revealed that in cells expressing Parkin with S65A or S65E mutations, Mfn1 and VDAC1 cannot be degraded effectively, and the mitochondrial outer membrane was likely more intact as indicated by the sustained

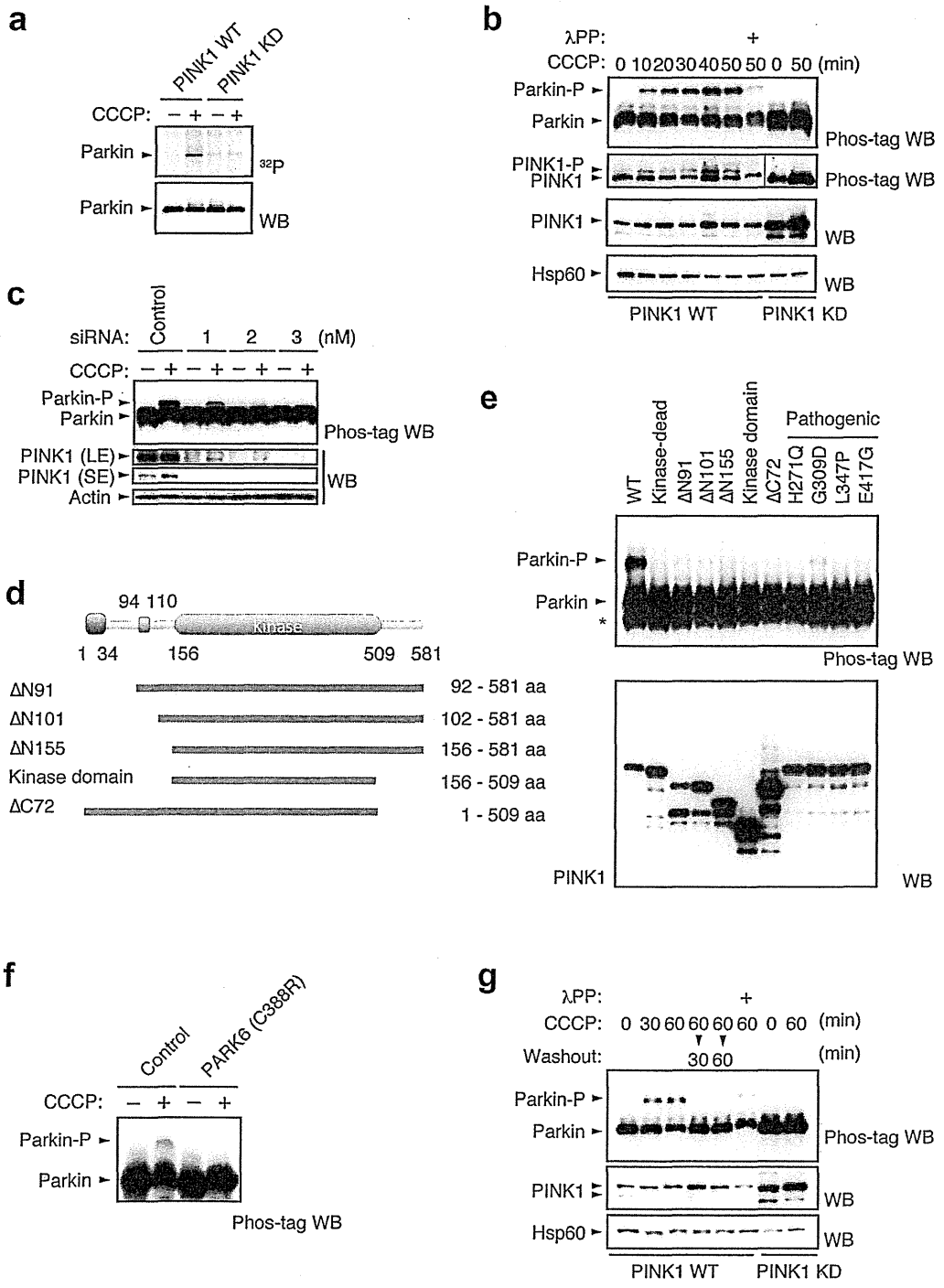

Figure 1 | PINK1-dependent phosphorylation of Parkin *in vivo*. (a) PINK1-FLAG WT or KD/HA-Parkin/*PINK1*$^{-/-}$ MEFs were labelled with [^{32}P] orthophosphate and treated with 30 μM CCCP for 1.5 hr. Phosphorylated Parkin was detected by autoradiography (^{32}P). Immunoprecipitated HA-Parkin was detected by Western blotting (WB) with anti-Parkin. (b) PINK1-FLAG WT or KD/HA-Parkin/*PINK1*$^{-/-}$ MEFs were treated with or without 30 μM CCCP for the indicated periods of time. Cell lysate was subsequently separated on a Phos-tag gel, followed by WB with anti-PINK1 or anti-Parkin antibodies (Phos-tag WB). Phosphorylated bands of Parkin and PINK1 were confirmed by their disappearance with lambda protein phosphatase (λPP) treatment. Mitochondrial Hsp60 was used as a loading control. (c) Suppression of endogenous PINK1 expression inhibits Parkin phosphorylation. HeLa cells stably expressing non-tagged Parkin were treated with the indicated concentrations of stealth siRNA duplex against PINK1 (Invitrogen) with or without 10 μM CCCP for 1 hr. Long- (LE) and short-exposure (SE) blot signals for PINK1 were shown. Actin was used as a loading control. (d) Truncated PINK1 mutants used in this study. Putative mitochondria-targeting sequence, 1–34 aa; transmembrane domain, 94–110 aa; kinase domain, 156–509 aa. (e) Full-length PINK1 is required for Parkin phosphorylation. *PINK1*$^{-/-}$ MEFs stably expressing non-tagged Parkin were transfected with various PINK1 constructs with C-terminal FLAG-tags. PINK1 expression was confirmed with anti-FLAG-HRP. (f) Human fibroblasts from a normal control and a *PARK6* case with a homozygous C388R mutation[44] were transfected with Parkin and were treated with or without 30 μM CCCP for 1 hr. (g) Cells treated with CCCP up to 60 min as in (b) were further incubated with fresh culture medium without CCCP for the indicated periods of time (Washout).

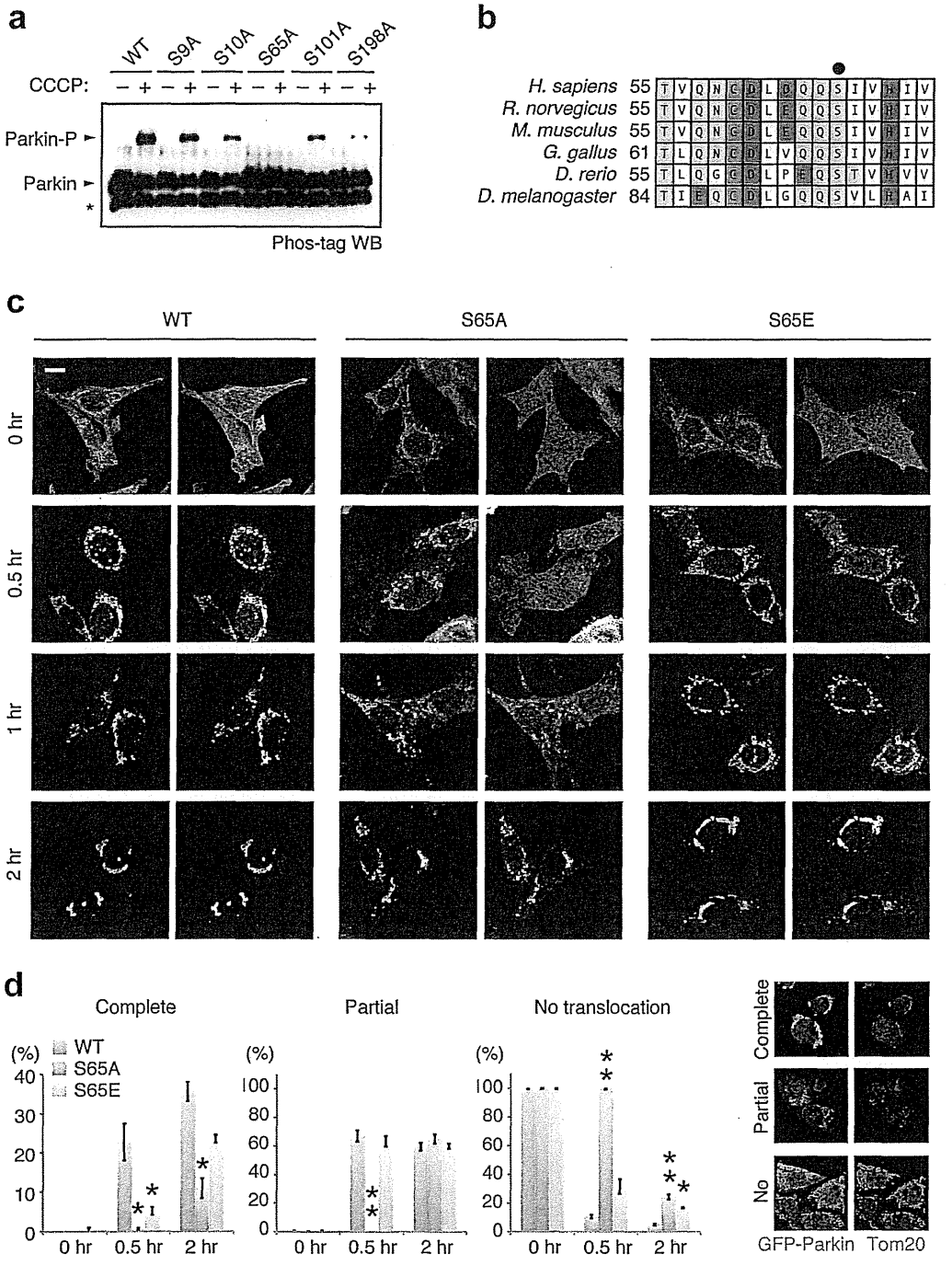

Figure 2 | Ser65 in the Ubl domain of Parkin is phosphorylated upon depolarisation of $\Delta\Psi$m. (a) Phos-tag Western blotting detected phosphorylation of Ser65. HeLa cells were transiently transfected with Parkin WT and a series of alanine mutants for the candidate phospho-residues followed by treatment with or without 20 μM CCCP for 1 hr. Cell lysates were analysed by Phos-tag Western blotting. An asterisk indicates degraded Parkin. (b) Alignment of the amino acid sequences surrounding Ser65 (marked by a black dot) from a variety of animal species. The numbers on the left correspond to the residue numbers of Parkin proteins. (c) Introduction of the S65A mutation delayed Parkin translocation to the depolarised mitochondria in PINK1 WT/GFP-Parkin/*PINK1*$^{-/-}$ MEFs. Cells retrovirally introduced with GFP-Parkin WT or its phospho-mutants (S65A and S65E) were treated with or without 30 μM CCCP for the indicated periods of time. GFP-Parkin and mitochondria were visualised with anti-GFP (green) and anti-Tom20 (red), respectively. Parkin signals are also shown as monochrome images. Scale bar = 10 μm. (d) Mitochondrial translocation efficiency of Parkin mutants. PINK1 WT/*PINK1*$^{-/-}$ MEFs stably expressing GFP-Parkin WT, S65A or S65E were treated as in (c). Cells expressing GFP-Parkin perfectly overlapped (Complete, examples are shown on the right), partially overlapped (Partial) or non-overlapped (No) with the Tom20 signal were counted. The data represent means ± SE from three experiments (n = 99–143 cells in each). ** $p < 0.01$, * $p < 0.05$ *vs.* WT at each time point.